The r-modes in accreting neutron stars with magneto-viscous boundary layers

Justin B. Kinney[1] and Gregory Mendell[2]
[1] *Cornell University, Ithaca, NY 14853*
[2] *LIGO Hanford Observatory, P.O. Box 159 S9-02, Richland, WA 99352*
(February 7, 2008)

We explore the dynamics of the r-modes in accreting neutron stars in two ways. First, we explore how dissipation in the magneto-viscous boundary layer (MVBL) at the crust-core interface governs the damping of r-mode perturbations in the fluid interior. Two models are considered: one assuming an ordinary-fluid interior, the other taking the core to consist of superfluid neutrons, type II superconducting protons, and normal electrons. We show, within our approximations, that no solution to the magnetohydrodynamic equations exists in the superfluid model when both the neutron and proton vortices are pinned. However, if just one species of vortex is pinned, we can find solutions. When the neutron vortices are pinned and the proton vortices are unpinned there is much more dissipation than in the ordinary-fluid model, unless the pinning is weak. When the proton vortices are pinned and the neutron vortices are unpinned the dissipation is comparable or slightly less than that for the ordinary-fluid model, even when the pinning is strong. We also find in the superfluid model that relatively weak radial magnetic fields $\sim 10^9\,\mathrm{G}\,(10^8\,\mathrm{K}/T)^2$ greatly affect the MVBL, though the effects of mutual friction tend to counteract the magnetic effects. Second, we evolve our two models in time, accounting for accretion, and explore how the magnetic field strength, the r-mode saturation amplitude, and the accretion rate affect the cyclic evolution of these stars. If the r-modes control the spin cycles of accreting neutron stars we find that magnetic fields can affect the clustering of the spin frequencies of low mass x-ray binaries (LMXBs) and the fraction of these that are currently emitting gravitational waves.

I. INTRODUCTION

The r-modes are oscillation modes that occur in rotating fluids due to the Coriolis effect. Great interest in these modes was generated after Andersson [1] and Friedman and Morsink [2] showed that gravitational-radiation backreaction tends to drive these modes unstable at all angular velocities. However, internal dissipation most likely completely suppresses this instability in all stars except neutron stars [1,2,3,4,5,6,7]. The r-mode instability in neutron stars is further complicated by the fact that the problem splits into two cases: superfluid neutron stars, with interior temperatures below approximately $10^9\,\mathrm{K}$, and within which the interior of a neutron star is expected to contain regions of superfluid neutrons mixed with lower concentrations of superconducting protons, normal electrons and other exotic particles, and ordinary-fluid neutron stars with interior tempertures above $10^9\,\mathrm{K}$. Furthermore, in a rotating neutron star the superfluid neutrons will form a dense array of quantized vortices, and if an interior magnetic field exists the superconducting protons (for type II superconductivity) will form a dense array of flux tubes (also called vortices in this paper). (See [8,9,10,11,12,13] for discussions of superfluidity in neutron stars.) A third case, not considered in this paper, is that in which the nucleons dissolve into a soup of up, down, and strange quarks, which results in a strange star, not a neutron star.

The regimes within which unstable r-modes can exist in neutron stars have been narrowed down as theoretical understanding has improved. First, Bildsten and Ushomirsky [14] showed that when a solid crust is present, the shear dissipation in the viscous boundary layer (VBL) that forms at the crust-core interface greatly suppresses the r-mode instability. Neutron stars are expected to form a solid crust for $\rho \lesssim 1.5 \times 10^{14}\,\mathrm{g/cm}^3$ and for tempertures below an approximate melting temperature of $T \cong 10^{10}\,\mathrm{K}$ [15,16]. This work was extended by Andersson *et al.* [17], Rieutord [18], Levin and Ushomirsky [19], Lindblom, Owen, and Ushomirsky [20], and Mendell [21]. Bildsten and Ushomirsky [14] also predicted that magnetic fields would be important in the VBL, for a magnetic field strength B and temperature T, when $B \geq 10^{11}\,\mathrm{G}\,(10^8\,\mathrm{K}/T)$. Mendell [21] confirmed this and showed that magnetic fields further suppress the instability in ordinary-fluid neutron stars. Second, Jones [22,23] and Lindblom and Owen [24] have shown that hyperon bulk viscosity further suppresses the instability above a temperature of 10^9K, while Haensel, Levenfish, and Yakovlev [25] have shown that superfluidity of the baryons tends to suppress hyperon bulk viscosity below 10^9K. In this paper we ignore hyperon bulk viscosity altogether. Finally, Wu, Matzner, and Arras [26] and Arras *et al.* [27] have shown that even if the r-modes are driven unstable, the saturation amplitude is likely to be very small.

However, the r-modes still remain important for the same reasons that sparked the initial interest in them.

First, it is still possible that they play a role in the spin-down of hot young pulsars [28]. Second, they could be reponsible for the clustering of spin frequencies inferred from the observations of low mass x-ray binaries (LMXBs) [29,30,31,32,33,17,34,35]. (However, note that some complications exist with the interpretation of the observations; see [36] and references therein.) Finally, even given the recent results, it is still possible that gravitational-waves from unstable small amplitude r-modes could be detected by enhanced or advanced narrow-banded gravitational-wave detectors. Theoretical understanding of the r-modes instability is far from complete, and thus more work is needed to understand these issues.

The purpose of this paper is to explore how the magneto-viscous boundary layer (MVBL) that forms at the crust-core interface in the presense of a radial magnetic field affects the dynamics of the r-modes in accreting neutron stars. Thus, this paper focuses on neutron stars with a solid crust ($T \leq 10^{10}\,\mathrm{K}$), and we assume that viscous dissipation in the MVBL is the dominant form of dissipation in these stars. Two models are considered: one assuming an ordinary-fluid interior; the other, which we refer to as the superfluid model, taking the core to consist of superfluid neutrons, type II superconducting protons, and normal electrons. First, we explore how dissipation in the MVBL at the crust-core interface governs the damping of r-mode perturbations in the fluid interior. This extends the work of Mendell [21] to the superfluid case. (Also, a minor coding error in Mendell [21] caused the MVBL damping times to come out about 53% percent too small and the critical angular velocities to come out about 11% too large. We give the corrected results in this paper.) Second, we evolve the r-mode amplitude, the angular velocity, and the temperature of the two models in time, accounting for accretion. We explore how the magnetic field strength, the r-mode saturation amplitude, and the accretion rate affect the cyclic evolution of these stars. This extends the work of Levin [33], Anderson, *et al.* [17], and Wagoner, Hennawi, and Liu [34] (see also Heyl [35]). We use the equations in Wagoner, Hennawi, and Liu [34] to evolve the models.

We show, within our approximations, that no solution to the magnetohydrodynamic (MHD) equations exists in the superfluid model when both the neutron and proton vortices are pinned. However, if just one species of vortex is pinned, we can find solutions. When the neutron vortices are pinned and the proton vortices are unpinned there is much more dissipation than in the ordinary-fluid model, unless the pinning is weak. When the proton vortices are pinned and the neutron vortices are unpinned the dissipation is comparable or slightly less than that for the ordinary-fluid model, even when the pinning is strong. We also find for the superfluid model that relatively weak radial magnetic fields $\sim 10^9\,\mathrm{G}\,(10^8\,\mathrm{K}/T)^2$ greatly affect the MVBL. We find that magnetic fields tend to make the critical angular velocity for the onset of the r-mode instability temperature independent and increase the dissipation rate, as Mendell [21] found in the ordinary-fluid case, though the effects of mutual friction tend to counteract the magnetic effects. Even when the magnetic field is zero, the correct scaling of the boundary layer thickness with the proton mass density is given here for the superfluid model for the first time.

When we evolve our two models in time we find that the critical angular velocity decreases with temperature sufficiently for all reasonable magnetic fields to produce the thermal run-away found by Levin [33]. (This happens even though magnetic fields tend to flatten the critical angular velocity vs. temperature curves. Wagoner, Hennawi, and Liu [34] have shown that if the critical angular velocity is (mostly) temperature independent then the r-mode amplitude and temperature oscillate with a period of hundreds to thousand of years, while the spin frequency of the star stays roughly constant.) Even with thermal run-way, Levin [33] and Anderson, *et al.* [17] showed that the r-mode instability can still produce clustering of the spin frequencies in LMXBs. If true, we find that magnetic fields can have important effects on this clustering. For radial fields of $B \gtrsim 10^{11}\,\mathrm{G}$ in the ordinary-fluid model or for $B \sim 10^9\,\mathrm{G}$ in the superfluid model the spin cycle of an LMXB becomes thinner, which would cause LMXBs with these fields to cluster into a narrower range of spin frequencies. Cumming, Zweibel, and Bildsten [37] have shown that buried fields in the crusts of accreting neutron stars must be less than $10^{11}\,\mathrm{G}$, while typical external fields in LMXBs are $10^{8-9}\,\mathrm{G}$. Furthermore, the interior magnetic field may be expelled during neutron star spindown or affected by accretion [38,39,40,41]. However, we know that neutron stars typically start out with large fields $\sim 10^{12}\,\mathrm{G}$. Since magnetic field evolution is uncertain, at some point it may be natural for the interior field to spend time at the values given here. If the magnetic field narrows the spin cycle of an LMXB, this increases the fraction of time it spends spinning down and radiating significant amounts of gravitational radiation. This, in turn, has an effect on the number of LMXBs that are currently radiating. Lowering the saturation amplitude or increasing the accretion rate produces the same effects, making it difficult to infer the interior field from current observations. However, the detection of gravitational waves from the r-modes of an accreting neutron star would determine the saturation amplitude (if the distance to source is known). In this case it might be possible to place limits on the interior magnetic fields of LMXBs with known accretion rates based on the observed allowed range of spin frequencies.

The next section reviews the Newtonian MHD equations for superfluid neutron stars. These reduce to the ordinary-fluid case when appropriate limits are taken. Sec. III finds an approximate solution to the MHD equations valid in the MVBL. Sec. IV presents the results of calculations for the MVBL damping times and the critical angular velocity, and discusses limits on the magnetic field and the MVBL length-scales. The models are evolved and the spin cycles of LMXBs are studied

in Sec. V. Conclusions are discussed and suggestions for future work are made in Sec. VI.

II. SUPERFLUID MHD EQUATIONS

The Newtonian MHD equations for a mixture of superfluid neutrons, type II superconducting protons, and normal electrons have been derived by Mendell [42]. The quantities in the equations represent smooth averages over volumes containing many vortices, based on the approach of Bekarevich and Khalatnikov [43] and as extended to neutron stars by Mendell and Lindblom [44], Mendell [45,46], and Lindblom and Mendell [47]. It is convenient to define the average and relative velocities, $\vec{v}$ and $\vec{w}$ respectively, in terms of the mass densities and velocities of the neutron and protons:

$$\rho\vec{v} = \rho_n\vec{v}_n + \rho_p\vec{v}_p, \tag{2.1}$$

$$\vec{w} = \vec{v}_p - \vec{v}_n. \tag{2.2}$$

For a star rotating uniformly in equilibrium with angular velocity $\vec{\Omega}$ ($\Omega = |\vec{\Omega}|$), the equations in Mendell [42] for small Eulerian perturbations (prefixed with a δ) can be written in the corotating frame as

$$\begin{aligned}\partial_t\delta\vec{v}+2\vec{\Omega}\times\delta\vec{v} = &-\vec{\nabla}\delta U + \frac{1}{\rho^2}\left(\frac{\partial\rho}{\partial\beta}\right)_p\delta\beta\vec{\nabla}p \\ &+\frac{1}{\rho}\left(\frac{\delta\vec{J}}{c}\times\vec{B}\right)+\frac{1}{\rho}\left[(\vec{\nabla}\times\delta\vec{\lambda}_p)\times\frac{e}{m_pc}\vec{B}\right] \\ &+\frac{1}{\rho}\vec{\nabla}\cdot(2\eta_e\delta\overleftrightarrow{\sigma}_e),\end{aligned} \tag{2.3}$$

$$\begin{aligned}\partial_t\delta\vec{w}+2\gamma\vec{\Omega}\times\delta\vec{w} = &-\vec{\nabla}\delta\beta+\frac{1}{\rho_p}\left(\frac{\delta\vec{J}}{c}\times\vec{B}\right) \\ &+\frac{1}{\rho_p}\left[(\vec{\nabla}\times\delta\vec{\lambda}_p)\times\frac{e}{m_pc}\vec{B}\right] \\ &+\frac{1}{\rho_p}\vec{\nabla}\cdot(2\eta_e\delta\overleftrightarrow{\sigma}_e)-\frac{\rho}{\rho_p}\delta\vec{F}_n,\end{aligned} \tag{2.4}$$

$$\partial_t\delta\vec{B} = \vec{\nabla}\times(\delta\vec{v}_e\times\vec{B}). \tag{2.5}$$

For simplicity, terms of order ρ_e/ρ_p have been ignored, and only the largest vortex force (dependent on $\vec{\lambda}_p$) has been retained. Dissipative effects due to the shear of the electron fluid, $\overleftrightarrow{\sigma}_e$, and the mutual friction force caused by electron scattering off the neutron vortices, $\vec{F}_n$, are included. The mutual friction force is given by [46]

$$\delta\vec{F}_n = 2\Omega\gamma\mathcal{B}_n\left[\delta\vec{w}-\frac{\vec{\Omega}(\vec{\Omega}\cdot\delta\vec{w})}{\Omega^2}\right], \tag{2.6}$$

where $\mathcal{B}_n$ is the mutual friction coefficient. In Eqs. (2.3) and (2.4) δU and $\delta\beta$ are related to the perturbed pressure, gravitational potential, and chemical potentials in the star but play no further role in this paper (see Lindblom and Mendell [47]). In Eqs. (2.4) and (2.6) γ is a dimensionless factor defined in Lindblom and Mendell [48] that arises due to the "entrainment" effect that occurs due to strong interactions between neutrons and protons [49,10,12]. When entrainment occurs the mass currents of the neutrons and protons are given in terms of the superfluid velocities by,

$$\vec{M}_n = \rho_{nn}\vec{v}_n + \rho_{np}\vec{v}_p, \tag{2.7}$$

$$\vec{M}_p = \rho_{np}\vec{v}_n + \rho_{pp}\vec{v}_p. \tag{2.8}$$

The coefficients, $\rho_{nn}, \rho_{np}, \rho_{pp}$ form what is called the mass density matrix. These are related to the ordinary mass densities and the entrainment factor γ by,

$$\rho_{nn} = \rho_n - \rho_{np}, \tag{2.9}$$

$$\rho_{pp} = \rho_p - \rho_{np}, \tag{2.10}$$

and

$$\rho_{np} = \frac{\rho_n\rho_p(1-\gamma)}{\rho}. \tag{2.11}$$

Next, note that Easson [50] calculates that the ratio of the magnetic diffusion time-scale to the viscous diffusion time-scale in a typical neutron star is roughly $10^{14}(10^8\,\mathrm{K}/T)^4$. Thus, the electrical conductivity of the electrons in the core and the crust is approximated as infinite; magnetic diffusion plays no role for the temperatures and time-scales of interest in this paper, and is ignored in Eq. (2.5). (See Mendell [21] for further disscusion of this issue.) Finally, e is the absolute value of the charge of the electron, m_p is the mass of the proton, and c is the speed of light.

The MHD limit is valid for studies of oscillations with phase velocities much less than the speed of light, frequencies much less than the plasma and cyclotron frequencies, and large conductivities. Under these circumstances the above equations, along with the mass conservation laws and equations of state, completely determine the dynamics of system. All the other vector fields of interest are determined in terms of $\delta\vec{v}$, $\delta\vec{w}$, and $\delta\vec{B}$. Specifically, for phase velocities much less than the speed of light, the displacement current can be ignored in Amperes law, and the current density is given by

$$\delta\vec{J} = \frac{c}{4\pi}\vec{\nabla}\times\delta\vec{B}. \tag{2.12}$$

For an infinitely conducting crust, there will also be a surface current density at the crust-core interface, given by

$$\delta\vec{I} = \frac{c}{4\pi}\left[\delta\vec{B}\times\hat{r}\right]_{r=R_c}, \tag{2.13}$$

where R_c is the radius of the core. For frequencies much less than the plasma and cyclotron frequency, the perturbed charge density is neglibible, and the perturbed electrical current density is so small that the electron velocity is approximately $\delta\vec{M}_p/\rho_p$ [45,42]. Using Eqs. (2.1)-(2.2) and Eqs. (2.8)-(2.11) this can be written as

$$\delta\vec{v}_e = \delta\vec{v} + \frac{\rho_n}{\rho}\gamma\delta\vec{w}. \tag{2.14}$$

Finally, when the above approximations hold and the conductivity is high, electrons (being the least massive charge carrier) respond to make the Lorentz force on them negligible, and the electric field is given by

$$\delta\vec{E} = -\frac{\delta\vec{v}_e}{c}\times\vec{B} - \frac{\vec{v}}{c}\times\delta\vec{B}. \tag{2.15}$$

Turning to the vortex force in Eqs. (2.3) and (2.4), this force is due to the underlying array the proton vortices (much smaller forces due to neutron vortices are ignored in this paper). It is given in terms of the vector vortex "chemical potential" λ^a (basically the energy per unit length needed to increase the number of proton vortices by one in direction a). Mendell [45,42] shows that this force is given by

$$\left[(\vec{\nabla}\times\delta\vec{\lambda}_p)\times\frac{e}{m_pc}\vec{B}\right] \cong -\left(\frac{\delta\vec{J}}{c}\times\vec{B}\right) + \frac{2m_p}{h}\left\{\left[\vec{\nabla}\times\delta(\varepsilon_p\frac{\vec{B}}{B})\right]\times\frac{e}{m_pc}\vec{B}\right\}. \tag{2.16}$$

The first term on the right side of this equation is not an approximation. It occurs in the exact form of the proton vortex force, and it always cancels the Lorentz force ($\propto \delta\vec{J}\times\vec{B}$) in Eqs. (2.3) and (2.4). For this reason, Alfvén waves do not occur in an exotic type II superconducting proton, normal electron plasma. Instead, these waves are replaced by cyclotron-vortex waves (see Mendell [42] and the next section). In the second term on the right side of Eq. (2.16), ε_p is the energy per unit length of a proton vortex. Small corrections to this term have been ignored (See Mendell [42]). Finally, throughout this paper note that $B = |\vec{B}|$.

III. APPROXIMATE MAGNETO-VISCOUS BOUNDARY LAYER SOLUTIONS

Approximate solutions to the superfluid MHD equations are found in this section. The ordinary-fluid limit of the solutions is also found. The equilibrium magnetic field is assumed to be arbitrary (for now) except that it is static in the corotating frame, and it is restricted such that no equilibrium electrical currents exist. This implies the equilibrium structure of the star is unchanged by the presence of the magnetic field. To facilitate the manipulation of tensor quantites, a rotating coordinate basis will be used, and indices will be raised and lowered using the flat-space metric tensor in spherical coordinates. In this basis, the equilibrium velocity is $v^a = \Omega\phi^a$. Following the notation of previous studies, note that Latin indices are space indices, except where it is understood that n, p, e, o, and c refer to neutrons, protons, electrons, ordinary, and the crust respectively.

Let δv^a, δw^a, and δB^a be the standard r-mode solution valid in the bulk of the core where viscous and magnetic forces are small compared to the Coriolis force. (As explained at the end of the last section, note that the magnetic forces are due entirely to the proton vortex force in the superfluid model.) By definition, the words "standard r-mode solution" mean the r-mode solution that would exist in the fluid core, if no solid crust were present. For the purposes of this paper, these solutions are also taken to be the lowest order form of the standard solution, when the solution is expanded in powers of the angular velocity. The standard r-mode solution is already known from previous studies of the r-modes. Note that δB^a is approximately zero, and is taken to be exactly zero in the standard r-mode solution. Furthermore, Lindblom and Mendell [48] show that $\delta w^a = 0$ at lowest order, and thus the lowest order superfluid r-mode solution is identical to the lowest order ordinary-fluid solution described in previous r-mode papers. (In general, see reference [48] for the standard r-mode solution in the notation used in this paper.) However, because of the solid crust, boundary conditions must be applied to the tangential components of the velocities at the crust-core interface. An ordinary viscous fluid cannot slip at a perfectly rigid boundary, and superfluid vortices cannot move if perfectly pinned at the boundary. However, electrons can slip at a conducting boundary. When fluids or vortices cannot slip at a boundary this causes a boundary layer to form. In the boundary layer the magnitudes of the viscous, magnetic, and Coriolis forces become comparible. Mutual friction forces can be important too. Thus, all these forces have effects on the structure of the boundary layer. When both viscous and magnetic forces exist we refer to the boundary layer as a MVBL.

Let $\delta\tilde{v}^a$, $\delta\tilde{w}^a$, and $\delta\tilde{B}^a$ be the corrections that must be added to the standard r-mode solution to enforce the tangential boundary conditions at the crust-core interface. The problem in this section reduces to finding solutions for the corrective quantities, $\delta\tilde{v}^a$, $\delta\tilde{w}^a$, and $\delta\tilde{B}^a$. Since the total fields are $\delta v^a + \delta\tilde{v}^a$, $\delta w^a + \delta\tilde{w}^a$, and $\delta B^a + \delta\tilde{B}^a$, and the equations are linear, the corrective quantities obey the same equations as the standard quantities, Eqs. (2.3)-(2.5). However, approximations that hold true for the corrective quantities in the MVBL are made when solving for these quantities that differ from the approximation made when finding the standard quantities. (This is done such that total solution is approximately valid inside and outside the MVBL.)

The main assumption, following the work of Lindblom, Owen, and Ushomirsky [20] and references therein, is that the boundary conditions force the corrective quantities to rapidly change in the radial direction. Thus, it is assumed that terms involving radial derivatives of the corrective quantities dominate the angular derivatives of these quanties, and dominate any derivative of all other quantities. (For certain angles, certain caveats must be added to this statement. These angles are discussed in Secs. IV.) By construction, the ratio of radial derivative terms kept to the terms dropped will be the ratio of the core radius to the boundary-layer length-scales. Thus, the main assumption is valid as long as the boundary layer length-scales are much less that the core radius.

Thus, it is possible to find approximate equations for the corrective quantities, $\delta\tilde{v}^a$, $\delta\tilde{w}^a$, and $\delta\tilde{B}^a$ by taking the following steps. First, let all perturbed quantities in the corotating frame have time dependence $\exp(i\kappa\Omega t)$, where κ is a constant that gives the mode frequency in terms of Ω. Second, note that since in the standard solution δv^r, δw^r, and δB^r vanish everywhere, mass is conserved at the boundary and the divergence of the magnetic field is zero if the radial components, $\delta\tilde{v}^r$, $\delta\tilde{w}^r$, and $\delta\tilde{B}^r$ also vanish. Finally, of the spacial derivative terms, only the highest order radial derivitives acting on the corrective quantities are kept, all other spacial derivative terms are dropped. Taking these steps, the resulting equations are as follows. First, Eq. (2.5) becomes,

$$\delta\tilde{B}^a = -\frac{i}{\kappa\Omega}B^r\partial_r\delta\tilde{v}_e^a. \tag{3.1}$$

Substituting this, Eq. (2.16), and Eq. (2.6) into Eq. (2.3) and Eq. (2.4) gives

$$\rho(i\kappa\Omega\delta\tilde{v}^\theta - 2\Omega\cos\theta\sin\theta\delta\tilde{v}^\phi)/\rho_p = \mathcal{F}\partial_r^2\delta\tilde{v}_e^\theta, \tag{3.2}$$

$$\rho(i\kappa\Omega\delta\tilde{v}^\phi + 2\Omega\cot\theta\delta\tilde{v}^\theta)/\rho_p = \mathcal{F}\partial_r^2\delta\tilde{v}_e^\phi, \tag{3.3}$$

$$\begin{aligned} &i\kappa\Omega\delta\tilde{w}^\theta - 2\gamma\Omega\cos\theta\sin\theta\delta\tilde{w}^\phi \\ &\quad + (2\gamma\Omega\rho\mathcal{B}_n/\rho_p)\delta w^\theta = \mathcal{F}\partial_r^2\delta\tilde{v}_e^\theta, \end{aligned} \tag{3.4}$$

$$\begin{aligned} &i\kappa\Omega\delta\tilde{w}^\phi + 2\gamma\Omega\cot\theta\delta\tilde{w}^\theta \\ &\quad + (2\gamma\Omega\rho\mathcal{B}_n/\rho_p)\delta w^\phi = \mathcal{F}\partial_r^2\delta\tilde{v}_e^\phi, \end{aligned} \tag{3.5}$$

where

$$\mathcal{F} = -i\left[\frac{V_{\rm CV}^2}{\kappa\Omega}\left(\frac{B_r}{B}\right)^2 + \frac{i\eta_e}{\rho_p}\right]. \tag{3.6}$$

In this equation, $V_{\rm CV}^2$ is the square of the cyclotron-vortex wave speed, defined by [42]

$$V_{\rm CV}^2 \equiv \frac{\varepsilon_p B}{\Phi_0\rho_p}, \tag{3.7}$$

where the quantum of flux is $\Phi_0 \equiv hc/2e$, and η_e is the electron viscosity (and recall that ε_p was previously defined after Eq. [2.16]).

Equating the right sides of Eqs. (3.2) and (3.4), and the right sides of Eqs. (3.3) and (3.5), the components $\delta\tilde{w}^\theta$ and $\delta\tilde{w}^\phi$ are given algebraically by

$$\begin{aligned} &i\kappa\Omega\rho_p\delta\tilde{w}^\theta - 2\gamma\Omega\rho_p\cos\theta\sin\theta\delta\tilde{w}^\phi + 2\gamma\Omega\rho\mathcal{B}_n\delta w^\theta \\ &\quad = \rho(i\kappa\Omega\delta\tilde{v}^\theta - 2\Omega\cos\theta\sin\theta\delta\tilde{v}^\phi), \end{aligned} \tag{3.8}$$

and

$$\begin{aligned} &i\kappa\Omega\rho_p\delta\tilde{w}^\phi + 2\gamma\Omega\rho_p\cot\theta\delta\tilde{w}^\theta + 2\gamma\Omega\rho\mathcal{B}_n\delta w^\phi = \\ &\quad \rho(i\kappa\Omega\delta\tilde{v}^\phi + 2\Omega\cot\theta\delta\tilde{v}^\theta). \end{aligned} \tag{3.9}$$

Combining these with Eq. (2.14) shows that Eqs. (3.2) and Eqs. (3.3) are a 4th order system for $\delta\tilde{v}_e^\theta$ and $\delta\tilde{v}_e^\phi$.

In deriving the above equations a factor of $\cos^2\theta$ has been ignored in the mutual friction force term in Eq. (3.4). Also,

$$\delta\left(\frac{B^a}{B}\right) = \frac{\delta B^a}{B} - B^a\frac{B^b\delta B_b}{B^3}, \tag{3.10}$$

which appears in the proton vortex force, has been approximated as $\delta B^a/B$. In the final equations this corresponds to ignoring terms of the order $(B_r/B)^2(B^\theta/B^2)^2$, $(B_r/B)^2(B^\theta B^\phi/B^2)$, and $(B_r/B)^2(B^\phi/B)^2$. These rather crude approximations make the analysis much easier to understand. The equations and solutions without these approximation are given in the Appendix. (In the final analysis, all magnetic terms, included the ignored ones, vanish if B_r vanishes; B_r controls the magnetic effects on the MBVL. Thus keeping only the largest terms that depends on B_r is not too bad.)

The corrective boundary layer solution is then found by allowing all perturbative quantities to vary as $\exp[ik(R_c - r)]$ (recall R_c is the radius of the core). It is easy to show that solutions exist for

$$k_\pm = K_\pm\sqrt{\frac{\Omega}{\frac{V_{\rm CV}^2}{\kappa\Omega}\left(\frac{B_r}{B}\right)^2 + \frac{i\eta_e}{\rho_p}}}, \tag{3.11}$$

$$K_\pm = \sqrt{\frac{(\kappa \pm 2\cos\theta)[\kappa \pm 2\gamma\cos\theta - (2i\rho\gamma\mathcal{B}_n/\rho_p)]}{[(\rho_n\gamma + \rho_p)/\rho]\kappa \pm 2\gamma\cos\theta - 2i\gamma\mathcal{B}_n}}, \tag{3.12}$$

$$\delta\tilde{v}^\theta = \pm i\sin\theta\delta\tilde{v}^\phi, \tag{3.13}$$

$$\delta\tilde{w}^\theta = \pm i\sin\theta\delta\tilde{w}^\phi. \tag{3.14}$$

and

$$\delta\tilde{w}^\theta = \frac{\rho(\kappa \pm 2\cos\theta)}{\rho_p(\kappa \pm 2\gamma\cos\theta) - 2i\rho\gamma\mathcal{B}_n}\delta\tilde{v}^\theta. \tag{3.15}$$

Choosing solutions where $\mathrm{Im}(k_\pm) > 0$, so that the solution decays exponentially as $r \to 0$, the general solution of the equations is of the form

$$\delta\tilde{v}_e^\theta = [C_+ e^{ik_+(R_c-r)} + C_- e^{ik_-(R_c-r)}]e^{i\kappa\Omega t}. \qquad (3.16)$$

We choose to define $C_\pm$ as the constants that give $\delta\tilde{v}_e^\theta$. Once these are determined by the tangential boundary conditions at the crust-core interface, all other components and velocities are determined in terms of these constants.

It is easy to find the analogous solution for a mixture of ordinary-fluid neutrons, protons, and electrons. In this case, all the fluids act as a single fluid, and the equations for this case can be obtained from (3.2) and (3.3) by taking the following limits:

$$\begin{aligned} &\lambda_p^a \to 0, \\ &\rho_p \to \rho, \\ &\eta_e \to \eta, \\ &v_e^a \to v^a, \\ &V_{\rm CV}^2 \to V_{\rm A}^2, \end{aligned} \qquad (3.17)$$

where $V_{\rm A}^2$ is the square of the Alfvén wave speed, defined as

$$V_{\rm A}^2 \equiv \frac{B^2}{4\pi\rho}. \qquad (3.18)$$

This equation should be compared with Eq. (3.7) for $V_{\rm CV}^2$. Choosing solutions where $\mathrm{Im}(k_\pm^o) > 0$, so that the solution decays exponentially as $r \to 0$, the general solution for the ordinary-fluid equations is of the form

$$\delta\tilde{v}^\theta = [C_+ e^{ik_+^o(R_c-r)} + C_- e^{ik_-^o(R_c-r)}]e^{i\kappa\Omega t}, \qquad (3.19)$$

where

$$k_\pm^o = K_\pm^o \sqrt{\frac{\Omega}{\frac{V_{\rm A}^2}{\kappa\Omega}\left(\frac{B_r}{B}\right)^2 + \frac{i\eta}{\rho}}}, \qquad (3.20)$$

and

$$K_\pm^o = \sqrt{\kappa \pm 2\cos\theta}. \qquad (3.21)$$

These equations are exactly those obtained by Mendell [21].

We must now consider what the correct tangential boundary conditions are at the crust-core interface. In the ordinary fluid case it is the no-slip boundary condition for a viscous fluid

$$[\delta v^a + \delta\tilde{v}^a = (1-\mathcal{S})\delta v^a]_{r=R_c}. \qquad (3.22)$$

Following Levin and Ushomirsky [19], but introducing our own notation, we introduce the "slip factor" $\mathcal{S}$ into Eq. (3.22). This is a simplified way to account for the motion of the crust. When $\mathcal{S} = 1$ the crust is perfectly rigid, and no slipping of the fluids at the boundary is allowed. A value of $\mathcal{S} = 0$ would correspond to a fluid crust, in which case the corrective solutions vanish. However, a realistic crust is not a fluid and not perfectly rigid. Levin and Ushomirsky [19] found for a toy model that $0.05 \le \mathcal{S} \le 1$.

Note that in the superfluid case the simple no-slip boundary condition does not apply. The reasons are the neutron and protons are superfluid and thus can slip, and the electrons are conducting and thus can slip along the conducting crust too. Instead, the tangential boundary conditions at the crust-core interface are determined by the pinning of the neutron and proton vortices. However, if both are pinned then the problem is over-determined and no solution exist. The reason for this is that in our approximation scheme the only independent velocity is that of the electrons; the other velocities are determined algebraically in terms of the components of $\delta\vec{v}_e$. Thus, if both the neutron and protron vortices are pinned, the approximation scheme used here breaks down and either the MVBL becomes much more complicated or the r-modes are drastically changed.

However, if just one species of vortex is pinned, we can find solutions. (More realistically, such solutions probably hold if the pinning of one vortex species completely dominates over the other species.) Using the equations in the Appendix of Mendell [46] we find, for a particular species, that the smooth-averaged perturbed vortex core velocity is proportional to the perturbed mass current projected perpendicular to the equilibrium direction of the vortex array. Since the radial components of the velocities are zero, this amounts to applying the tangential boundary conditions to the mass currents themselves. Using Eqs. (2.7) and (2.8), pinning just one vortex species corresponds to the pinned-vortex boundary condition,

$$\left[\delta v^a + \frac{\rho_{nn}}{\rho_n}\delta\tilde{v}_n^a + \frac{\rho_{np}}{\rho_n}\delta\tilde{v}_p^a = (1-\mathcal{S})\delta v^a\right]_{r=R_c}, \qquad (3.23)$$

for pinned neutron vortices, and

$$\left[\delta v^a + \frac{\rho_{np}}{\rho_p}\delta\tilde{v}_n^a + \frac{\rho_{pp}}{\rho_p}\delta\tilde{v}_p^a = (1-\mathcal{S})\delta v^a\right]_{r=R_c}, \qquad (3.24)$$

for pinned proton vortices. We introduce the factor $\mathcal{S}$ again to account for slipping of vortices or motion of the crust. A value of $\mathcal{S} = 1$ corresponds to strong (perfect) pinning while a value of $\mathcal{S} = 0$ corresponds to no pinning. Small values of $\mathcal{S}$ correspond to weak pinning. Several studies imply that vortex pinning in neutron stars, in general, may be moderate or weak, [51,52,53] though certain configurations may result in increased pinning strength [54]. (Also see Ruderman, Zhu, and Chen [40] for a disscussion of pinning and vortex interactions in the core.)

Applying the no-slip or pinned-vortex boundary conditions give

$$C_\pm = -\frac{1}{2}\mathcal{S}\Lambda_\pm(\delta v^\theta \pm i\sin\theta\delta v^\phi), \qquad (3.25)$$

where

$$\Lambda_\pm = 1, \tag{3.26}$$

in the ordinary fluid case or when the proton vortices are pinned, and

$$\Lambda_\pm = \frac{[(\gamma\rho_n + \rho_p)/\rho]\kappa \pm 2\gamma\cos\theta - 2i\gamma\mathcal{B}_n}{(\rho_{np}/\rho_n)\kappa - 2i\gamma\mathcal{B}_n}, \tag{3.27}$$

when the neutron vortices are pinned. In this latter case, this factor represents the fact that since equal but opposite forces couple the neutrons to the charged fluids (via the entrainment effect and mutual friction) the accelerations and motions of these fluids are inversely proportional to their mass densities. Thus, the factor $\Lambda_\pm$ is quite large when the neutron vortices are pinned. In contrast, since the electrons move with the proton mass currents, $\Lambda_\pm$ is 1 when the proton vortices are pinned. Similarly, since all the fluids move together in the ordinary-fluid case $\Lambda_\pm$ is 1 in this case as well. Furthermore, note that δv^θ and δv^ϕ in Eq. (3.25) are the same for the superfluid and ordinary-fluid models because, as already pointed out, the lowest-order standard r-mode solutions are identical for these two cases. These components of the velocity in the corotating frame (with their time dependence cancelled) are

$$\delta v^\theta = -iAr^{m-1}\sin^{m-1}\theta e^{im\phi}, \tag{3.28}$$

$$\sin\theta\delta v^\phi = Ar^{m-1}\sin^{m-1}\theta\cos\theta e^{im\phi}. \tag{3.29}$$

As shown in previous papers, the viscous damping rate is given by integrating the shear over the core:

$$\frac{1}{\tau_v} = \frac{1}{2E}\int 2\eta\delta\sigma^*_{ab}\delta\sigma^{ab}d^3x, \tag{3.30}$$

where E is the energy of the mode as defined in e.g., Lindblom and Mendell [48], but limited to the core. The largest contribution to the integral comes from the radial derivatives of the corrective boundary layer velocities, so that in the superfluid case

$$\delta\sigma^*_{ab}\delta\sigma^{ab} = \frac{1}{2}R_c^2(|\partial_r\delta\tilde{v}^\theta_e|^2 + |\partial_r\sin\theta\delta\tilde{v}^\phi_e|^2), \tag{3.31}$$

ignoring terms smaller than these by a factor of the boundary layer length-scales over the core radius. Thus, it can be shown that the solutions presented in this section give a VBL damping time of

$$\tau_v = \frac{2\pi}{\eta_e\mathcal{S}^2\mathcal{I}}\frac{2^{m+3}(m+1)!}{m(2m+1)!!}\int_0^{R_c}\rho\left(\frac{r}{R_c}\right)^{2m+2}dr, \tag{3.32}$$

where

$$\mathcal{I} = \int_0^{2\pi}\int_0^{\pi}\Big[|\Lambda_+|^2|k_+|^2d_+(1-\cos\theta)^2 + |\Lambda_-|^2|k_-|^2d_-(1+\cos\theta)^2\Big]\sin^{2m-1}\theta d\theta d\phi. \tag{3.33}$$

Using the definition

$$k_\pm \equiv \frac{2\pi}{\lambda_\pm} + \frac{i}{d_\pm}, \tag{3.34}$$

the boundary layer thicknesses in Eq. (3.33) and boundary layer wavelengths are defined as

$$\lambda_\pm \equiv \frac{2\pi}{\mathrm{Re}(k_\pm)}, \tag{3.35}$$

$$d_\pm \equiv \frac{1}{\mathrm{Im}(k_\pm)}. \tag{3.36}$$

The results given here reduce to those given in Mendell [21] in the ordinary-fluid limit.

Before we study in detail how MVBL damping affects the r-modes, we note the following useful analytic expressions for τ_v when the mutual friction coefficient $\mathcal{B}_n$ is 0. For simplicity we choose $B = B_r =$ constant. This is unrealistic (and unphysical unless as many field lines enter the crust core interface as leave it) but Mendell [21] has shown that this simple model gives the same qualitative results as a more complicated dipole field. In this case, the factors next to $K_\pm$ in Eq. (3.11) and next to $K^o_\pm$ in Eq. (3.20) are independent of θ, and we can factor them out of the integral $\mathcal{I}$, giving us

$$\frac{1}{\tau_v} = \mathcal{S}^2\left[C_{OF}\mathrm{Re}\left(\sqrt{q_{OF}B_r^2 + i\Omega/T_{10}^2}\right) + D_{OF}\mathrm{Im}\left(\sqrt{q_{OF}B^2 + i\Omega/T_{10}^2}\right)\right], \tag{3.37}$$

for the ordinary-fluid model and

$$\frac{1}{\tau_v} = \mathcal{S}^2\left[C_{SF}\mathrm{Re}\left(\sqrt{q_{SF}B + i\Omega/T_8^2}\right) + D_{SF}\mathrm{Im}\left(\sqrt{q_{SF}B + i\Omega/T_8^2}\right)\right], \tag{3.38}$$

for the superfluid model. In these equations $q_{OF} \equiv 1/(4\pi\kappa\eta_0)$, and $q_{SF} \equiv \epsilon_p/(\Phi_0\kappa\eta_{e,0})$, where η_0 and $\eta_{e,0}$ are the temperature independent part of the viscosities such that $\eta = \eta_0(10^{10}\,\mathrm{K}/T)^2$ and $\eta_e = \eta_{e,0}(10^8\,\mathrm{K}/T)^2$. The rest of the constants, $C_{\ldots}$ and $D_{\ldots}$, reduce to integrals over the angular variables that can be done numerically. Furthermore, when mutual friction is added to the superfluid model we find the following holds to about 4 parts in 10^4:

$$\tau_v \to \tau_v + \frac{A_{SF}}{\mathcal{S}^2}\frac{T_8^2}{\Omega}\mathrm{Re}\left(\sqrt{q_{SF}B + i\Omega/T_8^2}\right). \tag{3.39}$$

We find the constant A_{SF} (which is positive and depends on $\mathcal{B}_n$) by fitting this formula to the results given by Eq. (3.32).

IV. BOUNDARY LAYER DAMPING TIMES AND THE CRITICAL ANGULAR VELOCITY

One goal this study is to deterine how magnetic fields change the cricital angular velocity needed for the onset of the r-modes instability via their effect on the MVBL damping rate in accreting neutrons stars, such as those in LMXBs. Bildsten and Ushomirsky [14] predicted that magnetic fields would be important when $B \geq 10^{11}\,\mathrm{G}\,(10^8\,\mathrm{K}/T)$ and this was confirmed by Mendell [21] for the ordinarly-fluid model. However, Cumming, Zweibel, and Bildsten [37] have shown that buried fields in the crusts of LMXBs are less than 10^{11}G, while typical LMXBs have external fields that are about 10^{8-9}G. A minor coding error in Mendell [21] caused the MVBL damping times to come out about 53% percent too small and the critical angular velocities to come out about 11% too large, without changing the qualitative results. In this section we present corrected results for the ordinary-fluid model and extend those results to the superfluid model.

As shown in previous studies, gravitational radiation emitted by the r-modes always tends to drive these modes unstable. The onset of the instability occurs when the dissipation rate equals the gravitational-radiation growth rate, τ_{GR}. Thus, for our models we calculate the critical angular velocity for the onset of the instability by solving

$$\tau_v = \tau_{GR}, \tag{4.1}$$

where τ_v is given by Eq. (3.32) [see also Eqs. (3.37)-(3.39)] and τ_{GR} for the r-modes is given by

$$\tau_{GR} = \tilde{\tau}_{GR}\left(\frac{\Omega_o}{\Omega}\right)^{2m+2}, \tag{4.2}$$

where $\Omega_o = \sqrt{\pi G\bar{\rho}}$, G is the Newtonian gravitational constant, and $\bar{\rho}$ is the average density of the star (see references [1,2,3,4,5]).

Attention is restricted to the case used in previous studies: the $m = 2$ r-mode for a $1.4M_\odot$ $n = 1$ polytrope, as described in, e.g., Lindblom, Mendell, and Owen [6], and Lindblom and Mendell [48]. Adoption of this model allows easy comparison with previous studies. (Note also that the $m = 2$ case is the most susceptible to the r-mode instability.) For this case, $\kappa_0 = 2/3$, the stellar radius is 12.53 km, and $\Omega_o = 8413\,\mathrm{s}^{-1}$. Note that the maximum angular velocity, where mass shedding occurs at the equator, is roughly $2\Omega_o/3$ (for any equation of state). The density at the crust-core boundary is given approximately by $1.5 \times 10^{14}\,\mathrm{g/cm}^3$ (see [15,16]). Using this density, the characteristic gravitational-radiation growth time is $\tilde{\tau}_{GR} = 4.25\,\mathrm{s}$ [20], the core radius is $R_c = 11.01\,\mathrm{km}$, the proton density at the boundary is $\rho_p = 6.6 \times 10^{12}\,\mathrm{g/cm}^3$, and the superfluid entrainment factor is $\gamma = 1.90498$ (for an entrainment parameter of 0.04, as defined in Lindblom and Mendell [48]). In general, the dimensionless mutual friction coefficient is given by [46,48],

$$\mathcal{B}_n = 5.1 \times 10^{-5}\frac{(\gamma-1)^2\rho_n\rho_p^{7/6}}{\rho^{1/2}(\gamma\rho_n+\rho_p)^{3/2}}. \tag{4.3}$$

Thus, at the crust-core boundary the mutual friction coefficient is $\mathcal{B}_n = 9.5 \times 10^{-5}$. Furthermore, the energy per unit length of a proton vortex is given in Mendell [46] and in a more convenient form in Mendell [42]. However, even the latter form depends on uncertain parameters that involve the superconducting transition temperature and the entrainment factor. Here, all these uncertainties will be put into a single parameter ε. In this case, ε_p can be written as:

$$\varepsilon_p = \varepsilon\rho_{p,6.6e12}. \tag{4.4}$$

For typical neutron star numbers

$$\varepsilon \cong 1.4 \times 10^6\,\frac{\mathrm{erg}}{\mathrm{cm}}, \tag{4.5}$$

though its exact value is uncertain. Values for the viscosities are also needed. The electron and ordinary-fluid viscosities are given by [55]

$$\eta_e = \left(1.35 \times 10^{19}\frac{\mathrm{g}}{\mathrm{cm}\cdot\mathrm{s}}\right)\rho_{1.5e14}^2 T_8^{-2}, \tag{4.6}$$

$$\eta = \left(2.73 \times 10^{14}\frac{\mathrm{g}}{\mathrm{cm}\cdot\mathrm{s}}\right)\rho_{1.5e14}^{9/4} T_{10}^{-2}. \tag{4.7}$$

Note that we define $\rho_{1.5e14} = \rho/(1.5 \times 10^{14}\,\mathrm{g}\cdot\mathrm{cm}^{-3})$, $T_8 = T/(10^8\,\mathrm{K})$ (and so on for other numeric subscripts thoughout the rest of this paper).

Finally, one important simplification must be pointed out. As discussed at the end of the last section, it is convenient to choose $B = B_r =$ constant. As already explained, this is unrealistic but should give the same qualitative results as a realistic field (see Mendell [21]).

Before finding the results for the critical angular velocity, it is easy to show that magnetic effects will be important for the superfluid model for the typical fields found in LMXBs. If the magnetic terms are larger than the viscous terms in Eq. (3.11) then magnetic effects on the MVBL length-scales will be important. Thus, the condition for this is

$$\frac{V_{\mathrm{CV}}^2}{\kappa\Omega} \geq \frac{\eta_e}{\rho_p}, \tag{4.8}$$

Using Eq. (3.7) in Eq. (4.8) yields the following lower bound on the magnetic field, such that magnetic effects dominate the MVBL properties:

$$B \geq (3.8 \times 10^9\,\mathrm{G})\kappa\Omega_{600\pi}\rho_{1.5e14}^2 T_8^{-2}\rho_{p,6.6e12}^{-1}\varepsilon_{1.4e6}^{-1}, \tag{4.9}$$

Thus, in the superfluid model radial magnetic fields $\sim 10^9\,\mathrm{G}\,(10^8\,\mathrm{K}/T)^2$, not untypical of the fields of LMXBs, can affect the MVBL. Though, as we will show, the effects of mutual friction tend to counteract the magnetic effects.

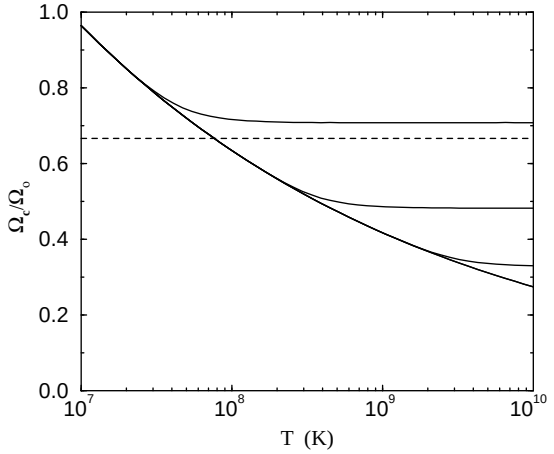

FIG. 1. Temperature dependence of the critical angular velocities for ordinary-fluid neutron stars for $B = 0$, 10^9 (indistinguishable from $B = 0$), 10^{10}, 10^{11}, and 10^{12} Gauss, from bottom to top.

For the physical parameters and restrictions just discussed, we solve Eq. (4.1) for the critical angular velocity Ω_c. The temperature dependence of the critical angular velocity is presented in Figs. 1-3. In these figures, the horizontal dashed line corresponds to $2\Omega_o/3$, which is the approximate maximum angular velocity for which mass-shedding occurs. Thus, the regions above this line are unphysical, and are kept only to illustrate the dependence of the curves for the range of magnetic field magnitudes typically found in neutron stars. Note that we extend the ordinary fluid curves into the superfluid region ($T \leq 10^9$K) and vice versa, given the uncertainties in the superfluid transition temperature.

Figure 1 shows the temperature dependence of the critical angular velocities for ordinary-fluid neutron stars for $B = 0$, 10^9 (indistinguishable from $B = 0$), 10^{10}, 10^{11}, and 10^{12} Gauss, from bottom to top. Overall, it is seen that magnetic fields increase the dissipation rate, raising the critical angular velocity, and flatten out the curves. The slip factor, $\mathcal{S}$, was set equal to 1 for all these curves. Smaller values of $\mathcal{S}$ lower these curves while preserving their shape.

Figures 2 and 3 show results for the superfluid model for the respective cases when just the neutron vortices are pinned or when just the proton vortices are pinned. The dotted lines are for $B = 0$, 10^9, 10^{10}, 10^{11}, and 10^{12} Gauss, from bottom to top when mutual friction is ignored ($\mathcal{B}_n = 0$), while the solid curves that diverge from these include the effects of mutual friction. The slip factor, $\mathcal{S}$, was set equal to 1 for all these curves. Smaller values of $\mathcal{S}$ lower these curves while preserving their shape. Thus, while many of these curves are far above the breakup velocity of the star, they can be moved into the physically allowed region by choosing a small value for $\mathcal{S}$, which corresponds to weak pinning of the vortices. As in the ordinary-fluid model, magnetic fields increase the

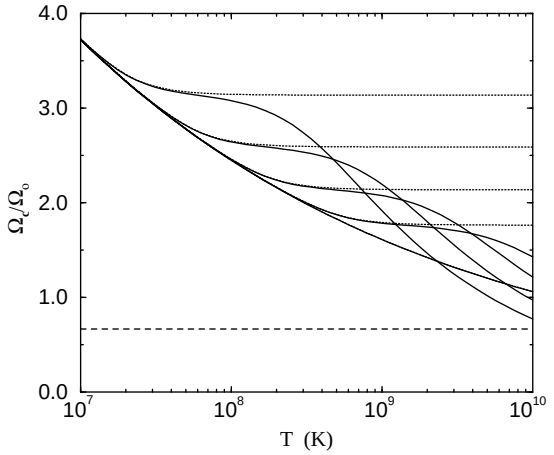

FIG. 2. Temperature dependence of the critical angular velocities for superfluid neutron stars with pinned neutron vortices for $B = 0$, 10^9, 10^{10}, 10^{11}, and 10^{12} Gauss, for dotted lines from bottom to top. Note that the dotted lines correspond to no mutual friction, while solid curves that diverge from these include mutual friction.

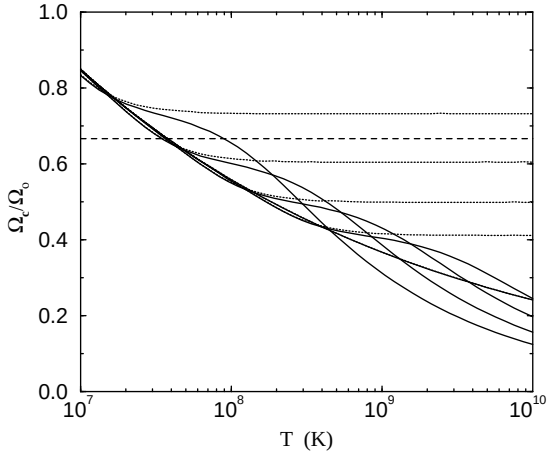

FIG. 3. Temperature dependence of the critical angular velocities for superfluid neutron stars with pinned proton vortices for $B = 0$, 10^9, 10^{10}, 10^{11}, and 10^{12} Gauss, for dotted lines from bottom to top. Note that the dotted lines correspond to no mutual friction, while solid curves that diverge from these include mutual friction.

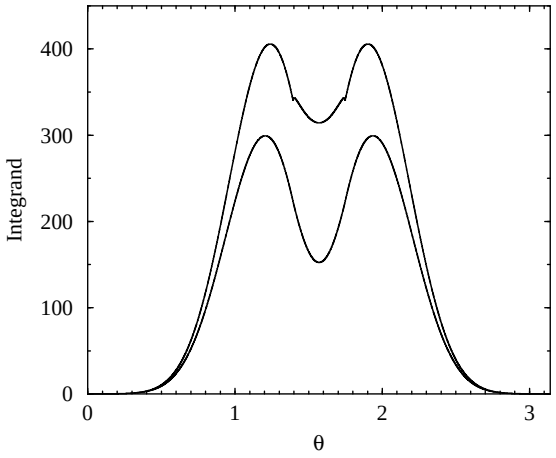

FIG. 4. Integrand that gives $\mathcal{I}$ for $T = 10^9$K, $B = 10^{10}$G, including mutual friction (lower curve) and excluding mutual friction (upper curve).

dissipation rate, raising the critical angular velocity, and flatten out the curves. However, it is also seen that mutual friction tends to counteract the magnetic effects for high temperatures or high fields.

The results shown here were computing numerically using τ_v as given by Eq. (3.32). However, we get the same results within a few tenths of a percent using Eqs. (3.37)-(3.39). For our models, the constants in these equations are $q_{OF} = 4.37 \times 10^{-16}\,\mathrm{s}^{-1} \cdot \mathrm{G}^{-2}$, $C_{OF} = 1.41 \times 10^{-6}\,\mathrm{s}^{-1/2}$, $D_{OF} = 1.56 \times 10^{-6}\,\mathrm{s}^{-1/2}$, $q_{SF} = 7.41 \times 10^{-7}\,\mathrm{s}^{-1} \cdot \mathrm{G}^{-1}$, while $C_{SF} = 0.261\,\mathrm{s}^{-1/2}$, $D_{SF} = 0.243\,\mathrm{s}^{-1/2}$, $A_{SF} = 0.0150\,\mathrm{s}^{1/2}$, for pinned neutron vortices, and $C_{SF} = 4.31 \times 10^{-5}\,\mathrm{s}^{-1/2}$, $D_{SF} = 1.05 \times 10^{-4}\,\mathrm{s}^{-1/2}$, for pinned proton vortices (we did not fit our data to determine A_{SF} for this case). Using these numbers and Eqs. (3.37)-(3.39), analytic expressions for τ_v for large B are

$$\tau_v = 33.9\,\mathrm{s}\,\mathcal{S}^{-2}B_{12}^{-1}, \tag{4.10}$$

for the ordinarly-fluid model, and

$$\tau_v = 0.141\,\mathrm{s}\,\mathcal{S}^{-2}B_9^{-1/2} + 4.85 \times 10^{-5}\,\mathrm{s}\,\mathcal{S}^{-2}T_8^2 B_9^{1/2}(\Omega_o/\Omega), \tag{4.11}$$

for the supefluid model when neutron vortices are pinned. Substituting these equations into Eq. (4.1) and using Eq. (4.2) gives the following analytic expressions for the critical angular velocities

$$\frac{\Omega_c}{\Omega_o} = 0.71\mathcal{S}^{1/3}B_{12}^{1/6}, \tag{4.12}$$

for the ordinarly-fluid model, while for the superfluid model with pinned neutron vortices we get

$$\frac{\Omega_c}{\Omega_o} = 1.76\mathcal{S}^{1/3}B_9^{1/12}. \tag{4.13}$$

when the first term on the right in Eq.(4.11) dominates, and

$$\frac{\Omega_c}{\Omega_o} = 9.74\mathcal{S}^{2/5}T_8^{-2/5}B_9^{-1/10}. \tag{4.14}$$

when the second term on the right in Eq.(4.11) dominates.

We now explain why our results scale with B, T, and Ω as they do. Note that in both the ordinary-fluid and superfluid models that the critical angular velocity becomes temperature independent for high temperatures (excluding mutual friction). However, one surprising result is that mutual friction actually lowers the damping rate. To understand the various cases we need to study the characteristic length-scales associated with the boundary layer.

The length-scales in the MBVL in the ordinary-fluid case have already been examined in Mendell [21]. Here we will consider the superfluid case. The characteristic length-scales of the MVBL are determined by examining Eq. (3.11) and the definitions of the length-scales given in Eqs. (3.35) and (3.36). Dropping subscripts for the purposes of discussion, since the MVBL damping rate is controlled by terms of the form $\eta|k|^2 d = \eta(4\pi/\lambda^2 + 1/d^2)d$, it would seem that the smallest length-scales would determine the damping rate. However, as found by Mendell [21], the ratio d/λ turns out to be more important when magnetic effects are important. Also, only real frequencies, $\kappa\Omega$, will be considered. This is valid either when the system is driven at a real frequency, or when the imaginary part of the frequency is small and can be ignored. (This is true for our models except near certain special angles, as will be explained.) Also, to further simplify the discussion, it will always be assumed that $\kappa > 0$.

First, consider Eq. (3.11) when B is less than the lower bounds given in Eq. (4.9). The viscous term dominates, and the boundary layer thicknesses and wavelengths are given to lowest order by

$$d_\eta = \frac{\lambda_\eta}{2\pi} = \frac{1}{|K_\pm|}\sqrt{\frac{2\eta_e}{\Omega\rho_p}}. \tag{4.15}$$

For typical neutron star numbers these length-scales are

$$d_\eta = \frac{\lambda_\eta}{2\pi} = \frac{47\,\mathrm{cm}}{|K_\pm|}\rho_{1.5e14}T_8^{-1}\Omega_{600\pi}^{-1/2}\rho_{p,6.6e12}^{-1/2}. \tag{4.16}$$

The effect of mutual friction is to only add small corrections to the above, and thus does not matter in this case. This equation agrees in form with the standard result, but differs from previous results by numerical factors of order unity due to the scaling with $|K_\pm|$, and more importantly, because the proper scaling with the proton mass density is given here for the superfluid case, for the first time. This increases the VBL thickness, and consequently the damping time, compared to previous estimates for the superfluid case, e.g., by a factor of about 4.5

compared to the calculation given by Lindblom, Owen, and Ushomirsky [20].

Mutual friction does matter for the case when B is greater than the lower bounds given in Eq. (4.9). However, we first consider the case when mutual friction can be ignored. In this case $K_\pm$ is either purely real or purely imaginary depending on the angle θ. Taylor expanding Eqs. (3.11) for this case the wave number is given by

$$k_\pm = K_\pm \sqrt{\frac{\kappa\Omega^2}{V_{\rm CV}^2}}\left[1 - \frac{i}{2}\frac{\eta_e}{\rho_p}\frac{\kappa\Omega}{V_{\rm CV}^2}\right]. \tag{4.17}$$

For the case of real $K_\pm$ the boundary layer length-scales to lowest order are

$$\frac{\lambda_B}{2\pi} = \frac{1}{|K_\pm|\kappa^{1/2}}\frac{V_{\rm CV}}{\Omega}, \tag{4.18}$$

which is basically the distance a cyclotron-vortex wave travels in one rotation, and

$$d_{B/\eta} = \frac{2}{|K_\pm|\kappa^{3/2}}\frac{V_{\rm CV}^3\rho_p}{\Omega^2\eta_e}. \tag{4.19}$$

The subscripts indicate whether these quanties depend on purely magnetic, or a ratio of magnetic to viscous quantities. Substituting in values for the parameters gives

$$\frac{\lambda_B}{2\pi} = \frac{33\,{\rm cm}}{|K_\pm|\kappa^{1/2}} B_{3.8e9}^{1/2}\Omega_{600\pi}^{-1}\varepsilon_{1.4e6}^{1/2}, \tag{4.20}$$

$$d_{B/\eta} = \frac{65\,{\rm cm}}{|K_\pm|\kappa^{3/2}} B_{3.8e9}^{3/2}\Omega_{600\pi}^{-2}T_8^2\varepsilon_{1.4e6}^{3/2}\frac{\rho_{p,6.6e12}}{\rho_{1.5e14}^2}. \tag{4.21}$$

For the case of imaginary $K_\pm$ the roles of λ and d become interchanged. Thus, for this case, the results are as in Eqs. (4.18)-(4.21) with

$$\begin{aligned} d &\to \frac{\lambda}{2\pi}, \\ \lambda &\to 2\pi d. \end{aligned} \tag{4.22}$$

It is apparent that for large B that the MVBL damping rate is dominated by terms of the type

$$\frac{1}{\tau_v} \sim \eta|k|^2 d \sim \eta\frac{d_{B/\eta}}{\lambda_B^2} \sim B^{1/2}. \tag{4.23}$$

This explains the regions where the damping rate becomes independent of the temperature and angular velocity, and the scaling of τ_v with $B^{-1/2}$ in the first term on the right side Eq. (4.11). Physically, the reason that magnetic fields increase the damping rate is that while magnetic forces increase the size of the boundary layer many wavelengths of cyclotron-vortex waves fit into the boundary layer thickness ($\lambda < d$) and there is a large amount of shear associated with these waves. (Similar explanations are given in Mendell [21] for the ordinary-fluid case.)

Attention will now be given to cases that occur near certain special angles in reference to Eq. (3.12). The angles are defined by

$$\kappa \pm 2{\rm cos}X_\pm = 0, \tag{4.24}$$

$$\kappa \pm 2\gamma{\rm cos}Y_\pm = 0, \tag{4.25}$$

$$\left(\frac{\rho_n\gamma + \rho_p}{\rho}\right)\kappa \pm 2\gamma{\rm cos}Z_\pm = 0. \tag{4.26}$$

The latter two of these angles are important to understanding the effects of mutual friction (and mutual friction smooths out singular behavior near these angles). For the models used in this paper, these angles are located at: $X_- = 1.23$, $X_+ = 1.91$, $Y_- = 1.39$, $Y_+ = 1.74$, $Z_- = 1.24$, and $Z_+ = 1.90$.

First, for θ near $X_\pm$, the small imaginary part of κ becomes important (in both the ordinary-fluid and superfluid models). As explained in Mendell [21], to understand this, make the replacement $\kappa \to \kappa + i/(\Omega\tau)$, and note that $\Omega\tau \gg 1$ for the situations of interest. It is seen that $k_\pm \propto \sqrt{i/(\Omega\tau)}$ and that the angular derivative $\partial k_\pm/\partial\theta$ becomes large near $X_\pm$ (infinite at $X_\pm$ when the imaginary part of κ is ignored). However, as shown in Mendell [21], these regions in the ordinary-fluid model make little contribution to the VBL damping rate. In the superfluid model, the proximity of $X_\pm$ to $Z_\pm$ tends to narrow the singular behavior near $X_\pm$. Thus, correcting for the small imaginary part of κ near $\theta = X_\pm$ is not done in this paper, nor has it been made in previous studies.

Now consider the case when mutual friction is included. Its effects are easiest to understand near the angles $Y_\pm$ and $Z_\pm$, which are special only in the superfluid model. The imaginary part of κ could also be important near these angles, but note that mutual friction effects are more important as long as $\tau > 1/(2\gamma\Omega\mathcal{B}_n)$. Thus, mutual friction effects dominates near $Y_\pm$ and $Z_\pm$ when the damping time is greater than the lower bound $\tau > 2.7\,{\rm s}/(\gamma\Omega_{600\pi}\mathcal{B}_{n,1.0e-4})$. It is found that this lower bound is valid for the results presented in this paper. Also, recall that mutual friction is only important for the case B is greater than the lower bound given in Eq. (4.9). With these caveats in mind, first consider the effects of mutual friction when θ is near $Y_\pm$. One can show that the characteristic MVBL length-scales are

$$d_{B/\mathcal{B}_n} = \frac{\lambda_{B/\mathcal{B}_n}}{2\pi} = \sqrt{\frac{2}{\kappa}}\sqrt{\frac{\rho_n\rho_p}{2\rho^2\mathcal{B}_n}}\frac{V_{\rm CV}}{\Omega}, \tag{4.27}$$

which for typical neutron star numbers is

$$\begin{aligned} d_{B/\mathcal{B}_n} = \frac{\lambda_{B/\mathcal{B}_n}}{2\pi} &= \frac{670\,{\rm cm}}{\sqrt{\kappa}} B_{3.8e9}^{1/2}\Omega_{600\pi}^{-1}\varepsilon_{1.4e6}^{1/2} \\ &\times \frac{\rho_{n,1.434e14}^{1/2}\rho_{p,6.6e12}^{1/2}}{\rho_{1.5e14}}\mathcal{B}_{n,1.0e-4}^{-1/2}. \end{aligned} \tag{4.28}$$

Next, for $\theta = Z_\pm$, the MVBL length-scales to lowest order are

$$d_{B\cdot\mathcal{B}_n} = \frac{\lambda_{B\cdot\mathcal{B}_n}}{2\pi} = \frac{\gamma}{(\gamma-1)}\sqrt{\frac{2}{\kappa}}\sqrt{\frac{2\rho^2\mathcal{B}_n}{\rho_n\rho_p}}\frac{V_{\rm CV}}{\Omega}, \qquad (4.29)$$

which for typical neutron star numbers is

$$d_{B\cdot\mathcal{B}_n} = \frac{\lambda_{B\cdot\mathcal{B}_n}}{2\pi} = \frac{(3.2\,{\rm cm})\gamma}{(\gamma-1)\kappa^{3/2}}\frac{B_{3.8e9}^{1/2}}{\Omega_{600\pi}}\varepsilon_{1.4e6}^{1/2} \times\frac{\rho_{1.5e14}}{\rho_{n,1.434e14}^{1/2}\rho_{p,6.6e12}^{1/2}}\mathcal{B}_{n,1.0e-4}^{1/2}. \qquad (4.30)$$

We see that the length-scales again depend on the distance a cyclotron-vortex wave travels in one rotation, but that $d = \lambda/2\pi$. Thus we do not have many wavelengths within the boundary layer, but only one wavelenth. We see that the length-scales near $Z_\pm$ are similar to the case when mutual friction is ignored. However, near $Y_\pm$ the length-scales are much larger than in the case when mutual friction is ignored. This reduces the dissipation rate and is the main reason that mutual friction reduces the critical angular velocities as shown in Figures 2 and 3. Also note, that when $d = \lambda/2\pi$ the dissipation varies as $\eta|k|^2 d \sim \eta/d$, and so the damping time varies as d/η. For d in Eqs. (4.28) and (4.30) we see that this implies $\tau_v \sim B^{1/2}T^2/\Omega$. Thus, we have explained the scaling of the mutual friction correction term with B, T, and Ω found empirically in Eq. (3.39) and used in Eqs.(4.11) and (4.14). The overall effect of mutual friction is shown in Fig. 4, which again shows that mutual friction lowers the dissipation rate, and smooths out singular behavior near the special angles considered here.

V. CYCLIC EVOLUTION OF ACCRETING NEUTRON STARS

We now turn our attention to the differential equations governing the spin cycles of accreting neutron stars. In the context of the r-modes, these cycles have been discussed by Levin [33], Anderson, *et al.* [17], Wagoner, Hennawi, and Liu [34], and Heyl [35]. Previously Wagoner [31] suggested that the spins of these stars could be limited by gravitational-radiation from an unstable mode, while Bildsten [32] proposed an alternative model in which the gravitational-radiation is generated due to an accretion-induced asymmetry of the star.

First, as in Owen *et al.* [5], we define the dimensionless r-mode amplitude α as the maximum perturbed fluid velocity at the equator of the star divided by ΩR. (Note that we do make corrections in this section for the fact the r-mode is confined to just the core of the star but that this does not change the definition of α.) Second, following the analysis of Wagoner, Hennawi, and Liu [34] (which builds on the work of Owen *et al.* [5] and Levin [33]), the following equations govern the evolution of the r-mode amplitude, α, the angular velcocity, Ω, and the temperature T:

$$\frac{1}{\alpha}\frac{d\alpha}{dt} = F_g - F_v + F_g K_c \alpha^2 - \frac{1}{2}F_a, \qquad (5.1)$$

$$\frac{1}{\Omega}\frac{d\Omega}{dt} = -2F_g K_c \alpha^2 + F_a, \qquad (5.2)$$

$$C(T)\frac{dT}{dt} = W_{\rm diss} + K_n\dot{M}c^2 - L_\nu(T). \qquad (5.3)$$

These equations, of course, are highly simplified in that they ignore differential rotation, assume infinite heat conduction, and so forth, but give a qualitative overview of how the evolution should proceed.

We now discuss the various terms in these equations. Heating due to dissipation is given by

$$W_{\rm diss} = \tilde{J}MR^2\Omega^2\alpha^2 F_v. \qquad (5.4)$$

The constant $\tilde{J}$ is defined in Eq. (3.4) of Owen *et al.* [5] and relates to the canonical angular momentum of the r-modes. Here we recompute this constant for r-modes confined to just the core of the star and find its value is $\tilde{J} = 0.01255$. The constant K_c, called Q in Owen *et al.* [5] and defined below their Eq. (3.4), is related to $\tilde{J}$ and the moment of inertia the star (which is unchanged even when the r-modes are confined to the core). However, since $\tilde{J}$ changes, K_c also changes, and we find $K_c = 0.072$. Next, note that Wagoner, Hennawi, and Liu [34] define $1 - K_j$ as the fraction of the canonical r-mode angular momentum that contributes to the total physical angular momentum of the star. In these equations we have adopted the case that the canonical angular momentum of the r-modes contributes zero physical angular momentum to the star, i.e., $K_j = 1$. We find in our case, as Wagoner, Hennawi, and Liu [34] find for the cases they study, that the exact value of K_j is not important to the results since the r-modes saturate quickly and no more physical angular momentum can go into them, if any at all does to begin with. Furthermore, Levin and Ushomirsky [56] show that the canonical angular momentum of the r-modes contributes zero physical angular momentum to the star for a toy model, further justifying our use of $K_j = 1$. Next, note that the above equations are valid only for small α. This is OK even when the mode saturates as long as the saturation amplitude is small. Several studies suggest the saturation amplitude is indeed small [26,27]. However, for comparison with earlier work we do consider a few cases where the saturation amplitude is $\alpha = 1$, and for these few case only we instead use Eq. (5) in Levin [33] to evolve Ω when $\alpha = 1$. As in Wagoner, Hennawi, and Liu [34], but using the MBVL damping rate which dominates for our models, we set

$$F_g = \frac{1}{\tau_{GR}}, \qquad (5.5)$$

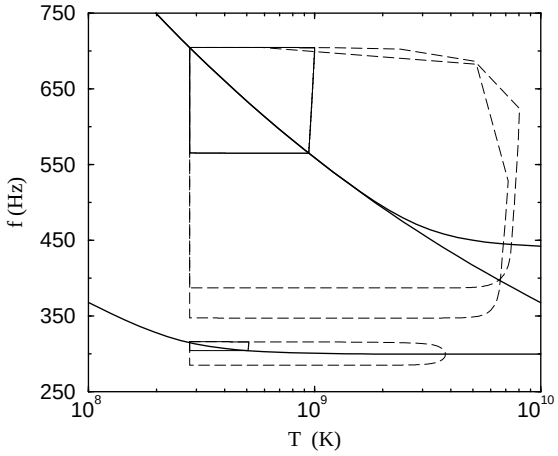

FIG. 5. Spin frequency vs. temperature evolution for ordinary-fluid neutron stars for $B = 0\,\mathrm{G}$ and $B = 10^{10}\,\mathrm{G}$ (both for $\mathcal{S} = 1.0$), and for $B = 10^{11}\,\mathrm{G}$ (for $\mathcal{S} = 0.1$). The curves are explained in the text.

where τ_{GR} is given by Eq. (4.2), while we set

$$F_v = \frac{1}{\tau_v}, \tag{5.6}$$

where τ_v is the MVBL damping time given by Eq. (3.32). The inverse accretion time-scale, F_a, is related to the accretion rate, $\dot{M}$, by

$$F_a = \left(\frac{1}{5\times 10^6 \mathrm{yr}}\right)\left(\frac{\dot{M}}{10^{-8} M_\odot/\mathrm{yr}}\right), \tag{5.7}$$

where the observed accretion rates in LMXBs are in the range $10^{-11} M_\odot/\mathrm{yr} \leq \dot{M} \leq 10^{-8} M_\odot/\mathrm{yr}$ [37]. We take the accretion rate to be constant. Even if the accretion rate were not constant, while the r-modes are saturated the accretion rate has little effect on the evolution. Note that heating due to accretion is proportional to the constant $K_n = 1\times 10^{-3}$ [34]. Finally, in Eq. (5.3) the heat capacity and neutrino cooling rates are given by [33,34,57],

$$C = 1.47\times 10^{38} \mathrm{erg}\cdot \mathrm{K}^{-1} T_8, \tag{5.8}$$
$$L_\nu = L'_{\mathrm{URCA}} T_8^8 + L'_{\mathrm{brem}} T_8^6, \tag{5.9}$$

for the ordinary-fluid case, and

$$C = 7\times 10^{36} \mathrm{erg}\cdot \mathrm{K}^{-1} T_8, \tag{5.10}$$
$$L_\nu = L'_{\mathrm{brem}} T_8^6, \tag{5.11}$$

for the superfluid case. The constants L'_{URCA} and L'_{brem} are given by [57],

$$L'_{\mathrm{URCA}} = 1.5\times 10^{32} \mathrm{ergs}^{-1}, \tag{5.12}$$
$$L'_{\mathrm{brem}} = 1.4\times 10^{30} \mathrm{ergs}^{-1}. \tag{5.13}$$

The results of evolving Eqs. (5.1)-(5.3) are the cyclic curves shown in Figs. 5-8. The monitonically decreasing smooth curve through the middle of each cycle is

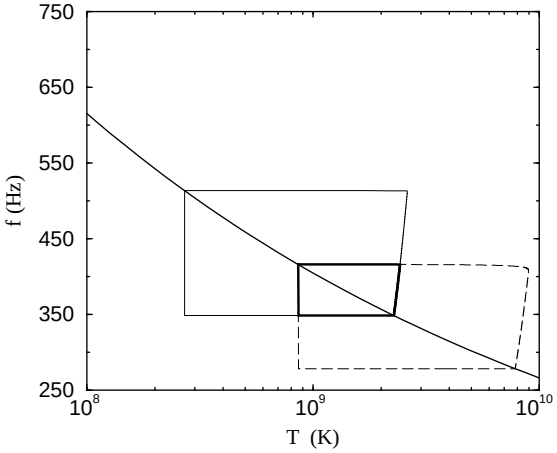

FIG. 6. Spin frequency vs. temperature evolution for superfluid neutron stars with pinned neutron vortices and for $B = 0\,\mathrm{G}$ and $\mathcal{S} = 0.01$. The curves are explained in the text.

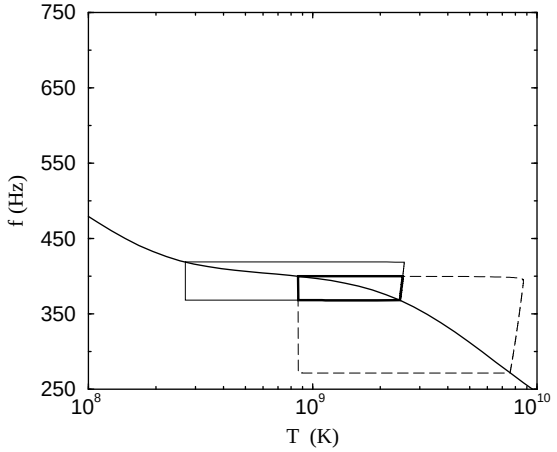

FIG. 7. Spin frequency vs. temperature evolution for superfluid neutron stars with pinned neutron vortices and for $B = 10^9\,\mathrm{G}$ and $\mathcal{S} = 0.005$. The curves are explained in the text.

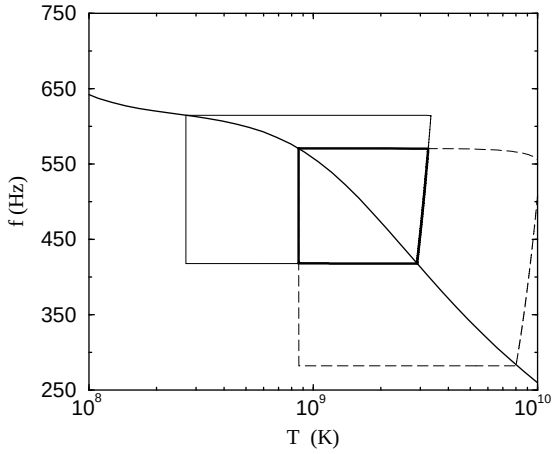

FIG. 8. Spin frequency vs. temperature evolution for superfluid neutron stars with pinned neutron vortices and for $B = 10^{10}\,\mathrm{G}$ and $\mathcal{S} = 0.01$. The curves are explained in the text.

the critical angular velocity curve. As time increases, a star progresses clockwise around the cycle. Note that for each cycle there is a maximum and minimum angular velocity and a maximum and minimum temperature. At the maximum angular velocity the r-mode becomes unstable at the minimum temperature, i.e., we define $\Omega_{\rm max} = \Omega_c(T_{\rm min})$. At the minimum angular velocity the r-mode becomes stable at the maximum temperature, i.e., we define $\Omega_{\rm min} = \Omega_c(T_{\rm max})$. We define the change in angular velocity by $\Omega_{\rm max} - \Omega_{\rm min} = \Delta\Omega$. We will describe some cycles as "thin" if $\Delta\Omega \ll \Omega_{\rm min}$, otherwise we will describe the cycle as "fat" if $\Omega_{\rm min} \ll \Omega_{\rm max}$. For each cycle the star goes through roughly 4 distinct stages. Each stage corresponds to one side of the roughly quadrulateral curve that corresponds to one cycle [58]. These stages have been previously discussed by Levin [33] and Anderson, *et al.* [17] (see also Heyl [35]). Here we extend their results to include the superfluid case, magnetic effects, and thin cycles. First we give typical numbers for our models. After this we discuss the figures in detail.

The first stage corresponds to the vertical left side of the cycle, which corresponds to the star spinning up by accretion with heating due to accretion balanced by cooling due to neutrino emission $K_n \dot{M} c^2 = L_\nu(T)$. Thus, the minimum temperture is related to the accretion rate by

$$T_{\rm min} = 2.8 \times 10^8\,\mathrm{K} \left(\frac{\dot{M}}{10^{-8} M_\odot/\mathrm{yr}}\right)^{1/8}, \qquad (5.14)$$

for the ordinary-fluid case, and

$$T_{\rm min} = 8.6 \times 10^8\,\mathrm{K} \left(\frac{\dot{M}}{10^{-8} M_\odot/\mathrm{yr}}\right)^{1/6}, \qquad (5.15)$$

for the superfluid case. The time-scale for accretion to spin up the star is given by solving Eq.(5.2) when F_a dominates:

$$t_{\rm spinup} = \frac{1}{F_a} \ln \frac{\Omega_{\rm max}}{\Omega_{\rm min}} = 5 \times 10^6\,\mathrm{yr} \left(\frac{10^{-8} M_\odot/\mathrm{yr}}{\dot{M}}\right) \ln\left(\frac{\Omega_{\rm max}}{\Omega_{\rm min}}\right). \qquad (5.16)$$

It will be useful to note that for thin cycles the spinup time is approximately,

$$t_{\rm spinup} \cong 5 \times 10^6\,\mathrm{yr} \left(\frac{10^{-8} M_\odot/\mathrm{yr}}{\dot{M}}\right) \left(\frac{\Delta\Omega}{\Omega_{\rm min}}\right). \qquad (5.17)$$

The second stage corresponds to the the top of the cycle. The beginning of this stage occurs when the r-mode becomes unstable and the mode amplitude grows to a saturation amplitude $\alpha_{\rm sat}$. This happens on the gravitational growth time-scale of

$$t_{\rm grow} = \frac{1}{F_g} \ln \frac{\alpha_{\rm sat}}{\alpha_{\rm min}} = 9.3\,\mathrm{hr} \left(\frac{600\pi/\mathrm{s}}{\Omega_{\rm max}}\right)^6 \ln\left(\frac{\alpha_{\rm sat}}{\alpha_{\rm min}}\right). \qquad (5.18)$$

As is done in Wagoner, Hennawi, and Liu [34], we assume a residual r-mode amplitude is continuously excited by stochastic processes and do not allow α to evolve below $\alpha_{\rm min} = 10^{-12}$. As the mode grows, viscous dissipation heats the star to a maximum temperture for which $\tilde{J} M R^2 \Omega^2 \alpha_{\rm sat}^2 F_v = L_\nu(T)$. Thus, the maximum temperature is determined by the saturation amplitude. If we overestimate F_v by replacing it with $F_g(\Omega_{\rm max})$ we find

$$T_{\rm max} \lesssim 5.0 \times 10^8\,\mathrm{K} \left(\frac{\alpha_{\rm sat}}{10^{-4}}\right)^{1/4} \left(\frac{\Omega_{\rm max}}{600\pi/\mathrm{s}}\right), \qquad (5.19)$$

for the ordinary-fluid case, and

$$T_{\rm max} \lesssim 1.9 \times 10^9\,\mathrm{K} \left(\frac{\alpha_{\rm sat}}{10^{-4}}\right)^{1/3} \left(\frac{\Omega_{\rm max}}{600\pi/\mathrm{s}}\right)^{4/3}, \qquad (5.20)$$

for the superfluid case. Next, we can solve Eq. (5.3) when the term with F_v dominates to get the characteristic time for dissipation to heat the star

$$t_{\rm heat} = \frac{1}{2 W_{\rm diss}} \left[C(T_{\rm max}) T_{\rm max} - C(T_{\rm min}) T_{\rm min})\right], \qquad (5.21)$$

If we make the approximations $T_{\rm max} \gg T_{\rm min}$ and $F_v \lesssim F_g(\Omega_{\rm max})$, estimates for this time-scale are

$$t_{\rm heat} \sim 96\,\mathrm{yr} \left(\frac{\alpha_{\rm sat}}{10^{-4}}\right)^{-3/2} \left(\frac{\Omega_{\rm max}}{600\pi/\mathrm{s}}\right)^{-6}, \qquad (5.22)$$

for the ordinary-fluid case, and

$$t_{\rm heat} \sim 69\,\mathrm{yr} \left(\frac{\alpha_{\rm sat}}{10^{-4}}\right)^{-4/3} \left(\frac{\Omega_{\rm max}}{600\pi/\mathrm{s}}\right)^{-16/3}, \qquad (5.23)$$

for the superfluid case. Note that this time-scale dominates the top of the evolution cycle.

The third stage occurs when angular-momentum radiated away as gravitational radiation spins down the star. Solving Eq.(5.2) when the term with F_g dominates gives

$$t_{\rm spindown} = \frac{\tilde{\tau}_{GR}}{12K_c\alpha_{\rm sat}^2}\left[\left(\frac{\Omega_o}{\Omega_{\rm min}}\right)^6 - \left(\frac{\Omega_o}{\Omega_{\rm max}}\right)^6\right]. \quad (5.24)$$

For thin cycles,

$$t_{\rm spindown} \cong 7.4\times10^5\,{\rm yr}\,\frac{\Delta\Omega}{\Omega_{\rm min}}\left(\frac{10^{-4}}{\alpha_{\rm sat}}\right)^2\left(\frac{600\pi/{\rm s}}{\Omega_{\rm min}}\right)^6, \quad (5.25)$$

while for fat cycles,

$$t_{\rm spindown} \cong 1.2\times10^5\,{\rm yr}\left(\frac{10^{-4}}{\alpha_{\rm sat}}\right)^2\left(\frac{600\pi/{\rm s}}{\Omega_{\rm min}}\right)^6. \quad (5.26)$$

This stage dominates the right side of the evolution cycles. Note that stages 2 and 3 begin at the same time. Because they have very different durations they can be studied separately.

The fourth stage begins when the star spins down to the critical angular velocity curve. The amplitude of the mode then decays away on the dissipation timescale

$$t_{\rm damp} = \frac{1}{F_v}\ln\frac{\alpha_{\rm sat}}{\alpha_{\rm min}} \sim 9.3\,{\rm hr}\left(\frac{600\pi/{\rm s}}{\Omega_{\rm min}}\right)^6\ln\left(\frac{\alpha_{\rm sat}}{\alpha_{\rm min}}\right), \quad (5.27)$$

where we have used $F_v \sim F_g(\Omega_{\rm min})$ during the damping to obtain the numerical estimate for this time-scale. The last stage is dominated by the time it takes the star to cool back to $T_{\rm min}$. Solving Eq. (5.3) when the L_ν dominates gives

$$t_{\rm cool} \cong \frac{(10^8\,{\rm K})^8}{6L'_{\rm URCA}}\left[\frac{C(T_{\rm min})}{T_{\rm min}^7} - \frac{C(T_{\rm max})}{T_{\rm max}^7}\right] \sim 4.9\times10^5\,{\rm yr}\left(\frac{10^8\,{\rm K}}{T_{\rm min}}\right)^6, \quad (5.28)$$

for the ordinary-fluid case, and

$$t_{\rm cool} \cong \frac{(10^8\,{\rm K})^6}{4L'_{\rm brem}}\left[\frac{C(T_{\rm min})}{T_{\rm min}^5} - \frac{C(T_{\rm max})}{T_{\rm max}^5}\right] \sim 4.0\times10^6\,{\rm yr}\left(\frac{10^8\,{\rm K}}{T_{\rm min}}\right)^4, \quad (5.29)$$

for the superfluid case. This stage dominates the bottom of the evolution curves. Note that stage 4 really coincides with stage 1 of the next cycle. Because they have somewhat different durations they can be studied separately.

Thus, as Levin [33], Anderson, *et al.* [17], and Heyl [35] conclude, we see that the time that the r-mode spends saturated (and thus actively radiating potentially detectable gravitational waves) is dominated by the spin-down time-scale, while the time that the r-mode spends with minimum amplitude (and thus radiating insignificantly) is dominated by the spinup time. Thus, defining r as the fraction of LMXBs in the active phase gives $r \cong t_{\rm spindown}/t_{\rm spinup}$, as in Levin [33]. For fat cycles, using Eqs. (5.16) and (5.26),

$$r \lesssim .072\left(\frac{10^{-4}}{\alpha_{\rm sat}}\right)^2\left(\frac{500\pi/{\rm s}}{\Omega_{\rm min}}\right)^6\left(\frac{\dot{M}}{10^{-8}M_\odot/{\rm yr}}\right), \quad (5.30)$$

where $\ln(\Omega_{\rm max}/\Omega_{\rm min})$ was treated as a factor of order unity. For thin cycles, using Eqs. (5.17) and (5.25),

$$r \lesssim .44\left(\frac{10^{-4}}{\alpha_{\rm sat}}\right)^2\left(\frac{500\pi/{\rm s}}{\Omega_{\rm min}}\right)^6\left(\frac{\dot{M}}{10^{-8}M_\odot/{\rm yr}}\right). \quad (5.31)$$

The first of these ratios is the same as what Levin [33] found, though scaled differently here. Note that for these equations we have scaled $\Omega_{\rm min}$ with the observed minimum value 250 Hz, rather than a typical value of 300 Hz to get upper bounds on r. We see that LMXBs spend about 6 times as much time radiating if their evolution is controlled by thin rather than fat cycles. However, current observations suggest that the mostly thinly clustered set of LMXBs probably have $\Omega_{\rm min}/2\pi \lesssim 250$ Hz and $\Omega_{\rm max}/2\pi \gtrsim 350$ Hz [29,30,32]. This case falls between the cases that Eqs. (5.31) and (5.30) are valid. Instead, using these numbers in Eqs. (5.16) and (5.24) gives $r = 0.18$. (It is possible of course that a subset of these might belong to an even more thinly clustered set of LMXBs; on the other hand, some pulsars have $\Omega/2\pi \gtrsim 600$ Hz indicating that some LMXBs have been able to spin up well beyond 350 Hz.) Levin [33] gives an estimate of 10–100 as the number of strongly accreting LMXBs in our galaxy. This would indicate that if the r-modes instability controls the cycles of LMXBs there is a good chance some LMXBs in the galaxy are currently radiating as long as the saturation amplitude is small. Levin [33] and Anderson, *et al.* [17] come to more pessimistic conclusions, based on a larger saturation amplitude. However, we should not be too optimistic either, and treat our values for r as upper bounds. Many LMXBs have accretion rates far lower than $10^{-8}M_\odot/{\rm yr}$, lowering the real chances that any LMXB currently radiates. Decreasing the size of the saturation amplitude increases the odds, but also makes the r-modes harder to detect. We discuss detectability again at the very end of this section. (Heyl [35], at the same time this paper was written, independently considered small saturation amplitudes. That paper estimates the number of LMXBs in the galaxy based on the observed number of millisecond pulsars and comes to a similar but perhaps more optimistic conclusion than presented here.)

We now discuss the cycles in each figure. In Fig. 5 curves are shown for the ordinary-fluid case. The dashed curves with large cycles are for $\dot{M} = 10^{-8}M_\odot\,{\rm yr}^{-1}$,

$\alpha_{\rm sat} = 1$, and $\mathcal{S} = 1$. The largest of these is for $B = 0\,{\rm G}$ and the slightly smaller cycle is for $B = 10^{10}{\rm G}$. The lower dashed curve showing a thin cycle is for $\mathcal{S} = 0.1$ and $B = 10^{11}{\rm G}$. This is the largest buried field that could exist in the crust of an LMXB [37], and we choose the slip factor to put this cycle within the observed range of spin frequencies of LMXBs. The thin solid lines are cycles for the same parameters as the dashed cycles, except for a more realistic saturation amplitude of $\alpha_{\rm sat} = 10^{-4}$. Recent studies indicate the saturation amplitude is small, and perhaps much smaller than 10^{-4} [26,27]. However, when the saturation amplitude is this small, the entire cycle moves into the superfluid region. Since the transition temperature is uncertain we do not exclude these curves as a possibility. The main conclusion drawn here is that only a very large fields can produce thin cycles in the ordinary-fluid case.

In Figs. 6-8 results are shown respectively for the superfluid model with pinned neutron vortices for $B = 0$, 10^9, and 10^{10} Gauss, and for $\mathcal{S} = 0.01$, $\mathcal{S} = 0.005$, and $\mathcal{S} = 0.01$. In each case, the slip factor is choose to put the curves within the observed range of spin frequencies observed in LMXBs. The case of pinned proton vortices would result in similar plots, but for different values of the slip factor. The dashed curves correspond to $\dot{M} = 10^{-8} M_\odot\,{\rm yr}^{-1}$ and $\alpha_{\rm sat} = 0.1$. The thick solid curves are for the same accretion rate, but $\alpha_{\rm sat} = 10^{-4}$. The thin solid curves are for $\dot{M} = 10^{-11} M_\odot\,{\rm yr}^{-1}$ and $\alpha_{\rm sat} = 10^{-4}$. The surprising main conclusion drawn here is that $B \sim 10^9$ has the largest effect on narrowing the cycles. This is because this value of B tends to flatten the critical anglular velocity curve in the relevant temperature range, while mutual friction causes it to vary with temperature again for larger B fields.

In general, lowering the saturation amplitude moves the lower right-hand corner of cycle to the left along the critical angular velocity curve, while increasing the accretion rate moves the upper left-hand corner of a cycle to the right along a critical angular velocity curve. Thus adjusting these can make a cycle more or less narrow, as can the magnitude of the magnetic field. This makes it hard to use current observations of LMXBs to place contraints on the internal physics of these stars. However, if a class of LMXBs with similar internal magnetic fields could be identified, one prediction is that weakly accreting LMXBs should exhibit a wider range of spins than strongly accreting LMXBs. In any case, magnetic fields can make the cycles thinner, and are thus potentially important to the explanation of the observed clustering of LMXB spin frequencies. Thus, if the appropriate magnetic fields are present in a class of LMXBs it will tend to make the cycles thinner and increase the number of currently radiating sources.

Given the uncertainties we cannot predict with any certainty if any LMXBs are currently radiating. However, no matter the odds, the detection of gravitational radiation from the r-modes is not ruled out for gravitational-wave detectors currently coming online (with their planned enhancements) as long as the saturation amplitude is not too small. Using Eq. (4.9) from Owen *et al.* [5] but correcting for the fact that in our models the r-modes are confined to the core, the average dimensionless gravitational-wave amplitude for a source a distance D away is,

$$h = 7.6 \times 10^{-27} \left(\frac{\alpha_{\rm sat}}{10^{-4}}\right) \left(\frac{\Omega}{600\pi/{\rm s}}\right)^3 \left(\frac{10\,{\rm Kpc}}{D}\right). \quad (5.32)$$

For this fudicial value of h, and assuming an integrated observation time of $10^7\,{\rm s}$, the optimal signal-to-noise (SNR) ratios are in the range $0.57 - 4.4$ for the LIGO noise curves given in Owen *et al.* [5]. (Since it is not possible to keep the detector optimally aligned with the source actual SNRs would be $5 - 10$ times smaller. However, advanced detectors can greatly improve the SNR in narrow frequency bands.)

Thus, assume that gravitational radiation is detected from an LMXB in our galaxy. The radiation can be identified as due to the r-mode instability if the observed frequency is in the correct ratio to the spin frequency of the LMXB. The measured gravitational-wave amplitude then determines the r-mode saturation amplitude (if the distance to the LMXB is known) which determines the right side of a spin cycle. If the accetion rate is known the left side of a spin cycle is known. It is unlikely to observe an LMXB along the top or bottom of a spin cycle. However, the maximum (or minimum) spin frequencies, which give the top (or bottom) of a spin cycle must be larger(or smaller) than the observed values for these. Thus, it might be possible to place limits on the interior magnetic fields of LMXBs with known accretion rates depending on how well the allowed range of spin frequencies can be determined.

VI. CONCLUSIONS

We have studied the r-modes in accreting neutron stars with magneto-viscous boundary layers for ordinary-fluid and superfluid models. The ordinary-fluid model is discussed in detail in Mendell [21]. We have shown, within our approximations, that no solution to the MHD equations exists when both the neutron and proton vortices are pinned. However, solutions can exist for cases when just one species of vortex is pinned. In these cases, the instability of the r-modes to gravitational-wave emission can limit the spins of neutron stars (though strongly pinned neutron vortices would completely suppress the instability). If both the neutron and proton vortices are completely unpinned, the results would be basically that found in Lindblom and Mendell [48] and Levin [33]. In general, magnetic fields increase the dissipation rate and flatten the critical angular velocity vs. temperature curves in both models. However, mutual friction in the superfluid model tends to counteract the magnetic

effects for high temperatures or high fields. Furthermore, if the r-mode instability controls the spin cycles of LMXBs we have shown several things. As in Levin [33] Anderson, *et al.* [17], and Heyl [35], we show that decreasing the saturation amplitude greatly increases the odds that at least one LMXB in our galaxy is currently radiating gravitational waves. We also show that making the spin cycles thinner further increases the odds by up to a factor of 6 compared to previous estimates. Finally, we show for the first time that magnetic fields, by flattening the critical angular velocity curves, make the spin cycles of LMXBs thinner and that this increases the fraction of time an LMXB spends radiating gravitational waves for $B \gtrsim 10^{11}\,\mathrm{G}$ in the ordinarly-fluid case and for $B \sim 10^{9}\,\mathrm{G}$ in the superfluid case. Previous studies predicated that probably no LMXBs are currently radiating in our galaxy, based on large values of the saturation amplitude $\alpha_{\rm sat}$. However, the subsequent studies of Wu, Matzner, and Arras [26] and Arras *et al.* [27] predict that α will be small. In any case, the previous studies agree with our result that the fraction of currently radiating LMXBs approaches one if $\alpha_{\rm sat} \lesssim 10^{-4}$ and if at least 10 strongly accreting LMXBs exist in our galaxy. However, if $\alpha_{\rm sat}$ is much larger than 10^{-4} then probably no LMXBs are currently radiating; if $\alpha_{\rm sat}$ is much smaller than 10^{-4} the r-modes may be undetectable. (Detection of a source in our galaxy is difficult, but not impossible for α as small as 10^{-4}.) However, if gravitational waves are detected from the r-modes of an accreting neutron star, it might be possible to place limits on the interior magnetic fields of LMXBs with known accretion rates based on their observed allowed range of spin frequencies.

Of course many caveats must be added to our conclusions. Our evolution graphs show that the fluids may go through a transition from superfluid to ordinary-fluid during the heating phase, and vice versa during the cooling phase. Vortices would probably not have time to migrate out of the core during the spindown phase, and thus superfluid effects could remain important above the transition temperature; but the details of what happens to the boundary layer during such a phase transition could become very messy. This is only one complication that we have ignored. The neutrons could be in the superfluid phase while the protons are in the normal phase (for example see Easson and Pethick [59]) and vice versa. Another possibility is that the protons could form a type I superconductor in the intermediate state rather than a type II superconductor in the vortex state [8]. We have also only studied the effects of mutual friction for one value of the entrainment factor; special values exist that would completely change our results [48]. Furthermore, we have ignored interactions between neutron and proton vortices (see [40]) and other dissipative effects, such as hyperon bulk viscosity [22,23,24,25]. Finally, nonlinear effects are ignored, such as the winding of magnetic fields lines, which could be important especially for $B \gtrsim 10^{10}\,\mathrm{G}$ [60,61,62]. The winding of field lines would introduce another temperature independent damping mechanism, and thus probably would complement our results. Clearly, an exact understanding of the r-mode instability is very complicated.

Finally, we remark on one final interesting question: If the r-modes control the spins of LMXBs, could the observation of gravitational waves from some of these objects distinguish between ordinary-fluid neutron stars, superfluid neutron stars, and strange stars? The recent study of Andersson, Jones, and Kokkotas [63] suggests that strange stars in LMXBs may emit persistent gravitational waves from saturated r-modes. We have shown that neutron stars in LMXBs, in agreement with Levin [33], Anderson, *et al.* [17], and Heyl [35], would emit gravitational waves for only part of their spin cycle. If we do not observe gravitational radiation from any LMXBs we probably do not learn much, since so many mechanisms can suppress the instability. However, if the r-modes are observed from some LMXBs, and the current theoretical understanding holds up, then the fraction of LMXBs that radiate would distinguish between neutron and strange stars. A detailed comparison between theory and observation would be needed to distinguish between ordinary-fluid and superfluid neutron stars, however. Obviously, further work is needed to understand the various possibilities.

ACKNOWLEDGMENTS

We wish to thank B. Owen, L. Lindblom, R. Wagoner, and R. Epstein for responding to email questions and helpful discussions concerning this work. JBK thanks the NSF REU program and Caltech for financial support and LIGO Hanford Observatory for hospitality extended to him while completing this work. This research was supported by NSF grant PHY-0096304.

APPENDIX: SUPERFLUID MVBL SOLUTION

We will now solve the corrective differential equations governing MVBL dissipation in a superfluid neutron star with arbitrary B-field and without our ignoring a factor of $\cos^2\theta$ in Eq. (3.4). For such a model, we obtain the system of differential equations:

$$
\begin{aligned}
A\delta\tilde{v}^{\theta} + B\delta\tilde{v}^{\phi} &= F\delta\ddot{\tilde{v}}^{\theta} + G\delta\ddot{\tilde{v}}^{\phi} + H\delta\ddot{\tilde{w}}^{\theta} + I\delta\ddot{\tilde{w}}^{\phi} \\
-B\delta\tilde{v}^{\theta} + A\delta\tilde{v}^{\phi} &= J\delta\ddot{\tilde{v}}^{\theta} + K\delta\ddot{\tilde{v}}^{\phi} + L\delta\ddot{\tilde{w}}^{\theta} + M\delta\ddot{\tilde{w}}^{\phi} \\
C\delta\tilde{v}^{\theta} + D\delta\tilde{v}^{\phi} &= F\delta\ddot{\tilde{v}}^{\theta} + G\delta\ddot{\tilde{v}}^{\phi} + H\delta\ddot{\tilde{w}}^{\theta} + I\delta\ddot{\tilde{w}}^{\phi} \\
-D\delta\tilde{v}^{\theta} + E\delta\tilde{v}^{\phi} &= J\delta\ddot{\tilde{v}}^{\theta} + K\delta\ddot{\tilde{v}}^{\phi} + L\delta\ddot{\tilde{w}}^{\theta} + M\delta\ddot{\tilde{w}}^{\phi}
\end{aligned}
$$

where

$$
\begin{aligned}
A &= i\rho\kappa \\
B &= -2\rho\cos\theta \\
C &= i\rho_p\kappa + 2\gamma\rho B_n\cos^2\theta
\end{aligned}
$$

$$
\begin{aligned}
D &= -2\rho_p\gamma\cos\theta \\
E &= i\rho_p\kappa + 2\gamma\rho B_n \\
F &= \frac{1}{\Omega}\left\{\frac{-i\rho_p V_{CV}^2}{\kappa\Omega}\left(\frac{B^r}{B}\right)^2\left[1-\frac{(B^\theta)^2}{B^2}\right]+\eta_e\right\} \\
G &= \frac{i\rho_p V_{CV}^2}{\kappa\Omega^2}\left[\frac{(B^r)^2 B^\theta B^\phi}{B^4}\right] \\
H &= \frac{\rho_n}{\rho}\gamma F \\
I &= \frac{\rho_n}{\rho}\gamma G \\
J &= G \\
K &= \frac{1}{\Omega}\left\{\frac{-i\rho_p V_{CV}^2}{\kappa\Omega}\left(\frac{B^r}{B}\right)^2\left[1-\frac{(B^\phi)^2}{B^2}\right]+\eta_e\right\} \\
L &= \frac{\rho_n}{\rho}\gamma J \\
M &= \frac{\rho_n}{\rho}\gamma K.
\end{aligned}
$$

As in the simplified case, this system of differential equations only has two linearly independent variables:

$$
\begin{aligned}
\delta\tilde{v}^\theta &= a\delta\tilde{w}^\theta + b\delta\tilde{w}^\phi \\
\delta\tilde{v}^\phi &= c\delta\tilde{w}^\theta + d\delta\tilde{w}^\phi
\end{aligned}
$$

where

$$
\begin{aligned}
a &= \frac{AC+BD}{A^2+B^2} \\
b &= \frac{AD-BE}{A^2+B^2} \\
c &= \frac{BC-AD}{A^2+B^2} \\
d &= \frac{AE+BD}{A^2+B^2}.
\end{aligned}
$$

This leaves us with two linearly independent systems of differential equations. Assuming the same exponential behavior for $\delta\tilde{v}$ and $\delta\tilde{w}$ as in the simplified model, we find

$$
k_\pm^2 = \frac{\beta \pm \sqrt{\beta^2 - 4\alpha\gamma}}{2\alpha}
$$

where

$$
\begin{aligned}
\alpha &= PS - QR \\
\beta &= PE + SC + DQ - DR \\
\gamma &= D^2 + CE
\end{aligned}
$$

and

$$
\begin{aligned}
P &= aF + cG + H \\
G &= bF + dG + I \\
R &= aJ + cK + L \\
S &= bJ + dK + M.
\end{aligned}
$$

[1] N. Andersson, Astrophys. J. **502**, 708 (1998).
[2] J. L. Friedman, and S. M. Morsink, Astrophys. J. **502**, 714 (1998).
[3] L. Lindblom, B. J. Owen, and S. M. Morsink, Phys. Rev. Lett. **80**, 4843 (1998).
[4] N. Andersson, K. Kokkotas, and B. F. Schutz, Astrophys. J. **510**, 846 (1999).
[5] B. J. Owen, L. Lindblom, C. Cutler, B. F. Schutz, A. Vecchio, and N. Andersson, Phys. Rev. D **58**, 084020 (1998).
[6] L. Lindblom, G. Mendell, and B. J. Owen, Phys. Rev. D **60**, 64006 (1999).
[7] L. Lindblom astro-ph/0101136; to appear in "Gravitational Waves: A Challenge to Theoretical Astrophysics", edited by V. Ferrari, J.C. Miller, and L. Rezzolla (ICTP, Lecture Notes Series) (2001).
[8] G. Baym, C. J. Pethick, and D. Pines, Nature **224**, 673 (1969).
[9] G. Baym, and C. J. Pethick, Ann. Rev. Nucl. Sci. **25**, 27 (1975); Ann. Rev. Astron. Astrophys. **17**, 415 (1979).
[10] M. A. Alpar, S. A. Langer, and J. A. Sauls Astrophys. J. **282**, 533 (1984).
[11] D. Pines, M. A. Alpar, Nature **316**, 27 (1985).
[12] J. A. Sauls, in Timing Neutron Stars, ed. H. Ögelman and E. P. J. van den Heuvel (Dordrecht: Kluwer), 457 (1988).
[13] R. I. Epstein, Astrophys. J. **333**, 880 (1988).
[14] L. Bildsten and G. Ushomirsky, Astrophys. J. **529**, L33 (2000).
[15] F. Douchin and P. Haensel, Phys. Lett. B **485**, 107, (2000); astro-ph/0006135.
[16] P. Haensel, in "Astrophysical Sources of Gravitational Radiation", Les Houches 1995, eds. J. A. Marck and J. P. Lasota (1995), astro-ph/9605164.
[17] N. Andersson, D. I. Jones, K. D. Kokkotas, and N. Stergioulas, Astrophys. J. **534**, L75 (2000); astro-ph/0002114.
[18] M. Rieutord, Astrophys. J. **550**, 442 (2001); Erratum Astrophys. J. **557**, 493 (2001); astro-ph/0003171.
[19] Y. Levin and G. Ushomirsky, MNRAS **322**, 515 (2001); astro-ph/0006028.
[20] L. Lindblom, B. J. Owen, and G. Ushomirsky, Phys. Rev. D **62** 084030 (2000); astro-ph/0006242.
[21] G. Mendell, Phys. Rev. D **64**, 044009 (2001).
[22] P. B. Jones, Phys. Rev. Lett. **86**, 1384 (2001).
[23] P. B. Jones, Phys. Rev. D **64**, 084003 (2001).
[24] L. Lindblom and B. J. Owen, Phys. Rev. D **65**, 084039 (2002); astro-ph/0110558.
[25] P. Haensel, K. P. Levenfish, and D. G. Yakovlev, A. & A. **381** 1080 (2002); astro-ph/0110575.
[26] Y. Wu, C. D. Matzner, and P. Arras Astrophys. J. **549**, 1011 (2001); astro-ph/0006123.
[27] P. Arras, E. E. Flanagan, S. M. Morsink, A. K. Schenk, S. A. Teukolsky, and I. Wasserman, submitted to Astrophys. J. (2002); astro-ph/0202345.
[28] B. J. Owen and L. Lindblom, Class. Quant. Grav. **19**, 1247 (2002); gr-qc/0111024.
[29] M. van der Klis, astro-ph/9710016 (1997).
[30] T. E. Strohmayer, astro-ph/0101160 (2001).
[31] R. V. Wagoner, Astrophys. J. **278**, 345 (1984).
[32] L. Bildsten, Astrophys. J. Lett. **501**, L89 (1998); astro-ph/9804325.
[33] Y. Levin, Astrophys. J. **517**, 328 (1999); astro-ph/9810471.

[34] R. V. Wagoner, J. F. Hennawi, and J. Liu, to appear in the Proceedings of the 20th Texas Symposium on Relativistic Astrophysics, (2001); astro-ph/0107229.
[35] J. Heyl, accepted for publication in Astrophys. J. Lett.; astro-ph/0206174.
[36] P. G. Jonker, M. Méndez, and M. van der Klis, submitted to MNRAS (2002); astro-ph/0204113.
[37] A. Cumming, E. Zweibel, and L. Bildsten, submitted to Astrophys. J. (2001); astro-ph/0102178.
[38] G. Srinivasan, D. Bhattacharya, A. Muslimov, A. Tsygan, Curr. Sci. **59**, 31 (1990).
[39] M. Ruderman Astrophys. J. **366**, 261 (1991); Astrophys. J. **382** , 587 (1991).
[40] M. Ruderman, T. Zhu, and K. Chen, Astrophys. J. **492**, 267 (1998); astro-ph/9709008.
[41] S. Konar, D. Bhattacharya, MNRAS **308**, 795 (1999); astro-ph/9812035.
[42] G. Mendell, MNRAS **296**, 903 (1998).
[43] I. L. Bekarevich and I. M. Khalatnikov, Sov. Phys. **13**, 643 (1961).
[44] G. Mendell, and L. Lindblom, Ann. Phys. **205**, 110 (1991).
[45] G. Mendell, Astrophys. J. **380**, 515 (1991).
[46] G. Mendell, Astrophys. J. **380**, 530 (1991).
[47] L. Lindblom, and G. Mendell, Astrophys. J. **421**, 689 (1994).
[48] L. Lindblom, and G. Mendell, Phys. Rev. D **61**, 104003 (2000).
[49] A. F. Andreev and E. P. Bashkin, Sov. Phys. JETP **42**, 164 (1976).
[50] I. Easson, Astrophys. J. **228**, 257 (1979).
[51] P. M. Pizzochero, L. Viverit, and R. A. Broglia, Phys. Rev. Lett. **79**, 3347 (1997); astro-ph/9709060.
[52] A. Sedrakian, I. Wasserman, and J. M. Cordes, Astrophys. J. **524**, 341 (1999); astro-ph/9801188.
[53] B. Link and C. Cutler astro-ph/0108281 (2001).
[54] M. Hirasawa and N. Shibazaki, astro-ph/0109196 (2001).
[55] C. Cutler, and L. Lindblom, Astrophys. J. **314**, 234 (1987).
[56] Y. Levin and G. Ushomirsky, astro-ph/9911295.
[57] R. V. Wagoner, private communication (2001).
[58] The code that generated the cycles used quality step-size control during the heating and spindown phases of the evolution. To speed up the code, once the cycle turned the lower right corner and the cooling phase had begun (indicated by the angular velocity reaching its minimum value and not changing) the code extrapolated to get the cooling and spinup phase of the curves. This was found to give the same cycles as using quality step-size control thoughout the evolution, except it makes the lower left corner of the cycles turn too sharply.
[59] I. Easson and C. J. Pethick, Astrophys. J. **227**, 995 (1979).
[60] H. .C. Spruit, A. & A. **341**, L1 (1999); astro-ph/9811007.
[61] L. Rezzolla, F. K. Lamb, and S. L. Shapiro, Astrophys. J. Lett. **531**, L141, (2000); astro-ph/9911188.
[62] L. Rezzolla, D. Marković, and S. L. Shapiro, Phys. Rev. D **64**, 104013 (2001); gr-qc/0107061; Phys. Rev. D **64**, 104014 (2001); gr-qc/0107062.
[63] N. Andersson, D. I. Jones, K. D. Kokkotas, astro-ph/0111582 (2001).